32 Body Surface Potential Mapping

Luigi de Ambroggi · Alexandru D. Corlan

P. W. Macfarlane, A. van Oosterom, O. Pahlm, P. Kligfield, M. Janse, J. Camm (eds.), *Comprehensive Electrocardiology*, DOI 10.1007/978-1-84882-046-3_32,

32.1 Introduction

Body-surface potential maps (BSPMs) present the distribution of cardiac potentials on the chest surface during the cardiac cycle. They provide the spatial as well as the temporal and amplitude components of cardiac electrical activity, whereas the ECG scalar waveforms present only the time–voltage variation in a given lead point.

When an excitation wavefront spreads through atrial or ventricular heart muscle, it generates bioelectric currents, which distribute themselves to all conducting tissues in the body. This wavefront is a thin layer of heart muscle separating resting from excited areas. For the sake of simplicity, reference is made to the "classical" electrical model [1], according to which an excitation front is considered to be equivalent to a uniform dipole layer, where the dipole axis is everywhere orthogonal to the front; moreover, the tissue resistivity is supposed to be homogeneous. According to this model, currents arise from the anterior aspect of the front, flow through the thorax, and finally point to the posterior aspect of the front. Figure 32.1 illustrates the distributions of the currents and potentials, in a horizontal thoracic section, arising from an excitation wavefront in the ventricular septum. The locations of the potential maximum and minimum on the thoracic surface are correlated with the topography and orientation of the wavefront. According to the traditional solid angle theory, a potential maximum in a given area on the chest surface indicates that an excitation wave is pointing toward that area; a potential minimum indicates that the posterior or negative aspect of the wavefront is seen from the area where the minimum is present.

However, the relationship between surface potential distribution and wavefront shape is sometimes very complex. In fact, the potential distribution at the surface depends on the location, number, and geometry of the wavefronts in the thorax, the geometry of the torso, and the inhomogeneities of the conducting medium (cardiac and extracardiac tissues). For example, several excitation waves may be travelling simultaneously through the right and left ventricle, giving rise to a complex distribution of currents and potentials. Also, when an excitation wave spreading from the endocardium reaches the epicardial surface, a hole appears in the advancing wavefront. Through this hole or "window," the currents reenter the heart. If a window is close to the chest wall, a new potential minimum appears on the thoracic surface, in addition to those already present. A similar hole appears in the excitation wavefront when a portion of ventricular wall cannot be activated, because of a local myocardial infarction. In this case too, a potential minimum appears on the chest surface in the region facing the infarcted area. A further cause of complexity arises from the fact that the dipole density is not uniform on the surface of the wavefront, in that a wavefront spreading along fibers generates more current per unit area than a wavefront spreading across fibers [2, 3].

During repolarization, currents proportional to transmembrane potential gradient from the M-cell region flow toward the epicardium and endocardium, the former being of higher amplitude [4, 5]. This amounts to numerous small dipoles distributed in the whole mass of the myocardium. The orientation of these dipoles remains mostly unchanged during repolarization, and their amplitudes change relatively synchronously. Localized repolarization changes further add to the complexity of the body-surface potentials in heart disease.

Every excitation wave and every portion of repolarizing tissue in the heart influence the potential distribution on the entire body surface. It follows that information on the electrical activity of the heart can be recorded not only from the points commonly explored by conventional ECG and VCG leads, but also from the entire body surface. BSPMs provide all the information available on the entire chest surface.

32.2 History

The first example of a potential map was published by A. Waller in 1889 [6], on the basis of 10–20 ECG recordings from the surface of the human body; the potential distribution resembled that which would have appeared if a dipole had been located in the heart. Later, a few attempts to determine surface potential distributions were made by several authors with rudimentary techniques.

In 1951, Nahum et al. [7] published the first description of isopotential line distribution on the thoracic surface at successive instants during the cardiac cycle in man. They did not detect the simultaneous presence of several maxima and minima but observed that the surface potential distribution was much more complicated than that likely to result from an equivalent dipolar generator. In the 1960s, Taccardi [8, 9] described the instantaneous distribution of heart potentials during ventricular activation in dogs and in normal human subjects. These investigations clearly showed that several potential

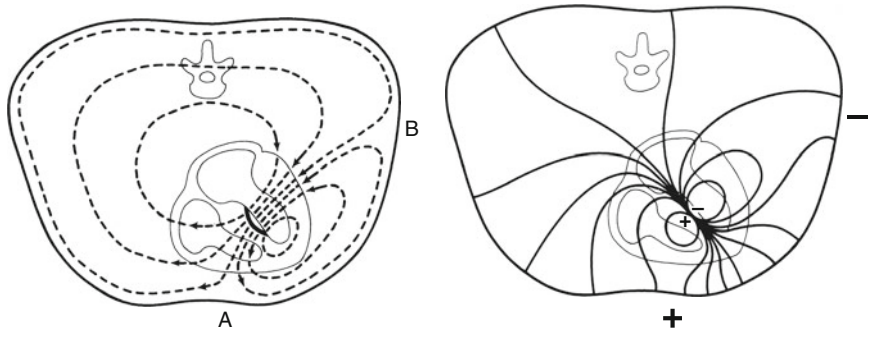

Figure 32.1

***Left*: Schematic drawing of a horizontal section of the human thorax illustrating the pathway of the currents, which arise from an excitation wavefront (solid line in septum) spreading through the septum in a left-to-right direction. A indicates the area where the current lines reach the surface; B indicates the area from which the currents dip into the thorax pointing to the posterior aspect of the wavefront. *Right*: Potential distribution in the same thoracic section and at the same instant. The plus sign indicates the location of the potential maximum on the surface (corresponding to point A); the minus sign indicates the location of the potential minimum (corresponding to point B).**

maxima and minima may be simultaneously present on the body surface during part of the QRS interval; moreover, an attempt was made to correlate the location of surface maxima and minima with the probable location of excitation wavefronts in the ventricles. The complexity of surface potential patterns, although not physically incompatible with a dipolar source, strongly suggested that a more complex electrical model of the heart should be adopted in order to account for the potential distributions found on the human and canine trunk.

Since then, BSPMs have been recorded from normal subjects (newborns and adults), cardiac patients, and experimental animals by many investigators in different countries.

32.3 Methods

Many lead systems have been used to record BSPMs throughout the world differing in the number of leads as well as in electrode location on the thorax. In theory, the optimal lead system should have a number of leads large enough to detect all details of the potential distribution on the torso surface. However, transformation methods have been proposed to estimate BSPM in a particular lead system from the BSPM data measured by using another lead system [10].

Techniques for recording, processing, and displaying the potential maps are illustrated in Chap. 31.

Different methods of analysis of BSPMs have been used to extract relevant information. These are described below.

32.3.1 Instantaneous BSPMs

The distribution of chest potentials in each instant of the cardiac cycle can be analyzed qualitatively, by visual inspection, or quantitatively by considering a number of numerical parameters relating to location, amplitude, and migration of potential maxima and minima.

32.3.2 Integral Maps

Since differences between maps of normal subjects and patients cannot easily be quantified by inspection of the sequence of instantaneous potential distributions, the potential–time integral maps have been considered. This approach has been proved to allow a reduction in the amount of data to be analyzed without substantial loss of information [11]. With this method, only a few maps are required to represent a cardiac cycle (QRS, ST-T, QRST, or other intervals for particular

purposes). In addition, this technique permits the calculation of average maps for groups of subjects without the need for time-phase alignment.

An approximation of the potential time integral, relating to a given interval of the cardiac cycle, is obtained by computing, at each lead point, the algebraic sum of all the instantaneous potential values throughout the interval considered, multiplied by the sampling interval. The values, expressed in mVms, are transferred to a diagram representing the thoracic surface explored, and isointegral contour lines can be drawn (Fig. 32.2).

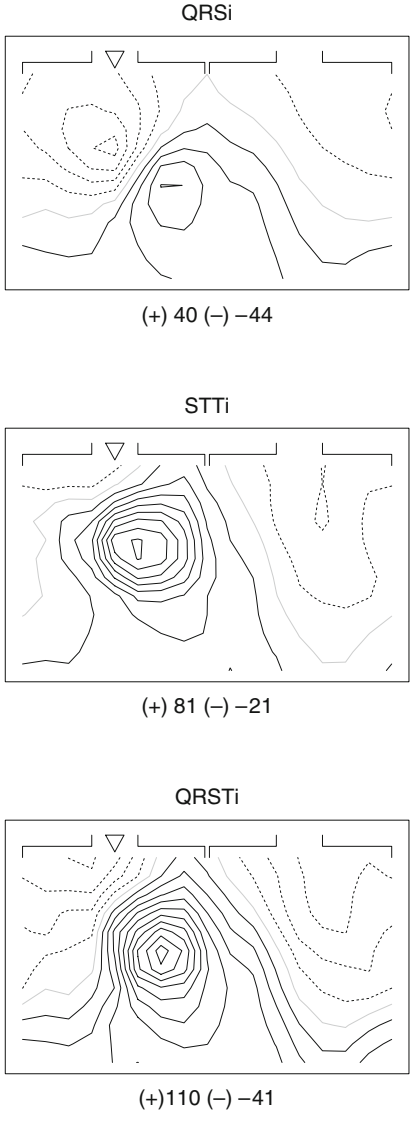

Figure 32.2

Integral maps in a normal subject during the QRS interval (*top*) ST-T interval (*middle*) and QRST interval (*bottom*). The left half of each map represents the anterior face of the thorax, the right half represents the posterior face. Continuous dark lines represent positive isointegrals, dashed lines represent negative isointegrals. The grey continuous line represents the zero integral line. The legend under each map indicates by (+) the maximum integral value on the respective map, by (–) the minimum integral value and (:) the gradient between isointegral lines, in 10 mVms.

32.3.3 Principal Component Analysis

Reduction of the information in body-surface ECG recordings can be achieved by decomposing individual integral maps or population-wide sets of recordings or the matrix of potentials in time over an interval (such as the ST-T) into components, which are independent of (noncorrelated to) each other. For example, singular value decomposition of the matrix of instantaneous repolarization potentials in time can be written as a sum of components each consisting of a potential distribution on the body surface, changing in time. The relative spatial distribution of the potentials of each component is constant, and the only thing that changes in time is the general amplitude of the component.

Figure 32.3 shows the first four components of the ST-T potentials in a normal subject. The first component contains normally over 75% of the potential amplitude, and is probably due to the general transmural gradient of the ventricular action potential. The second component is usually opposed (inversely correlated) to the QRS integral and likely corresponds to the repolarization gradient secondary to the depolarization sequence. The relative contribution of the first or

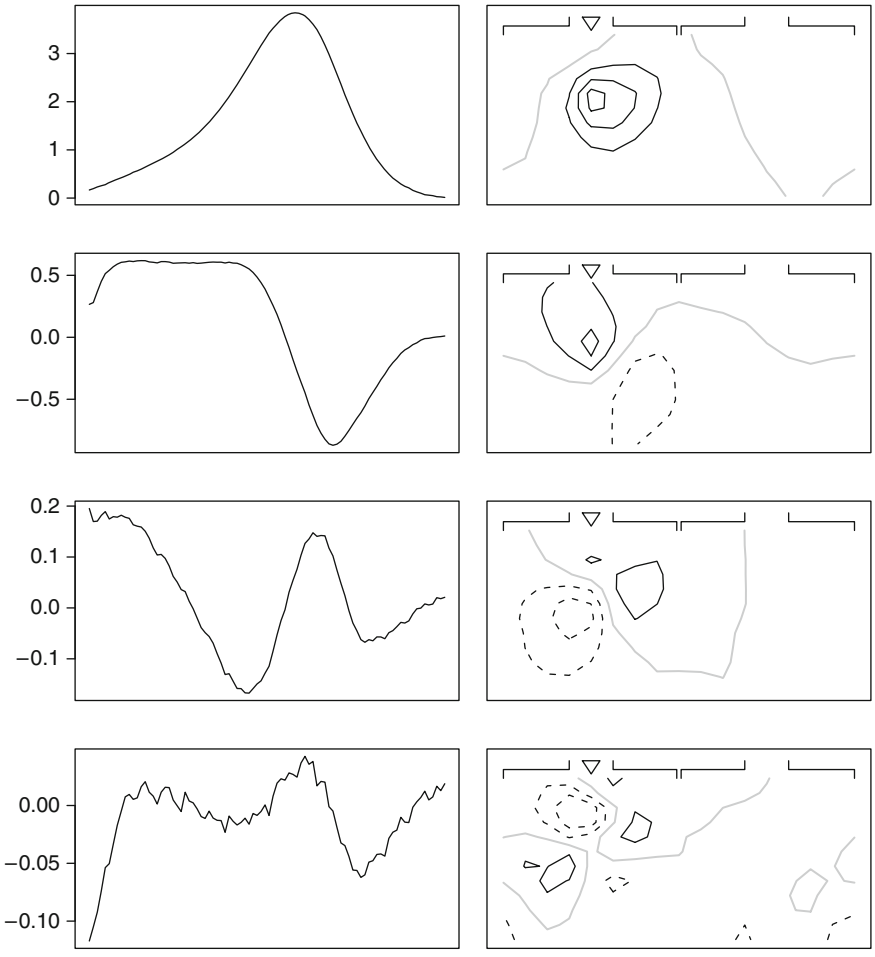

Figure 32.3

The first four components resulting from singular value decomposition of the matrix of instantaneous repolarization potentials versus time in a normal recording. Each component is represented by the body-surface potential distribution (*right*) (distance between isopotential lines is arbitrary) and the variation of its amplitude in time (*left*) (time on *x*-axis and relative amplitude on *y*-axis). The first component is at the *top*, the fourth at the *bottom*.

first two components to the repolarization potentials is decreased in most pathological states and may be indicative of the presence of arrhythmogenic repolarization heterogeneity.

Reduction of the information in body-surface ECG recordings to a few numerical indices can be achieved by analysing individual recordings or population-wide sets of recordings into components that are independent of (not correlated to) each other. One method is principal component analysis in which a set of signals, either instantaneous body-surface distributions at different instants in time, or time-based signals from different leads, or integral maps in a group of individuals are decomposed into eigenvectors (components, usually sets of potentials) and eigenvalues (numbers which quantify the contribution of each eigenvector to the general variability of the overall data). Ventricular repolarization is particularly suitable to this type of analysis, as most of the variability of normal repolarization potentials in most instants over the ST-T interval can be described by a single component.

32.3.4 Autocorrelation Maps

Autocorrelation (AC) maps are square matrices of values between -1.0 and 1.0, which represent the correlation coefficients of every pair of instantaneous potential distributions from a set of successive instants in time [12]. The same time interval appears on both coordinates of the map and the matrix is symmetrical with respect to the first diagonal. Values on the first diagonal are always 1.0, representing correlations of each instantaneous map with itself.

Autocorrelation maps reflect only phenomena taking place in the ECG source (myocardium) and are very little influenced by the geometry of the volume conductor (thorax) that connects it to the lead system [13]. AC maps are very sensitive to variations in the activation sequence. For example, Figs. 32.4 and 32.5 show recordings in two healthy individuals in whom the 12 lead ECGs and QRS integral maps look very much alike, but differences in the activation sequence are evident in the instantaneous potential maps, especially in the AC maps.

The AC map of the ST-T interval is normally quite close to 1 as the normal repolarization pattern shows little change, apart from the amplitude. The extent of change can be quantified by choosing the map at the peak of T (on the root mean square signal) as a reference map and calculating the average difference from one of the lines that goes through that instant on the AC map over the S-T peak and T peak-end intervals. We call these average differences the early and late repolarization deviation indices (ERDI and LRDI), respectively.

32.4 Normal Maps

32.4.1 Atrial Excitation and Recovery

At the onset of atrial excitation, a potential minimum is generally observed near the right sterno-clavicular joint, in the right supraclavicular region, or in the right mammary area (Fig. 32.6a) [14, 15]. The potential maximum or minimum is here defined as a point on the thoracic surface where the potential value is higher or lower in relation to all the surrounding points. Mirvis [16] did not observe a clear-cut minimum, but only a broad area of negative low-level potentials over the upper back and the right chest during the initial phase of atrial excitation. A potential maximum is initially located either in the right submammary area or in the lower sternal region (Fig. 32.6b). During the subsequent stages of atrial activation, the maximum moves leftward, gradually reaching the left mammary region, the left lateral chest wall and, in some cases, the dorsal region (Fig. 32.6c). The minimum moves slightly downward. During the leftward migration of the maximum, a secondary potential maximum sometimes appears on the left lateral wall of the thorax. The movement of the potential maximum from right to left is most likely correlated with the spread of the excitation wavefronts from the right to the left atrium.

During atrial recovery (Fig. 32.6d), surface potential maps resemble those recorded in the early stages of atrial excitation, but with reverse polarity [15–17]. A potential minimum is generally located on the sternal and left mammary region and a maximum on the right shoulder both in adults and infants. This finding suggests that repolarization advances through the atrial walls in approximately the same order as does excitation. This is in agreement with experimental data, demonstrating that the atrial regions that depolarize first are also the first to recover [18].

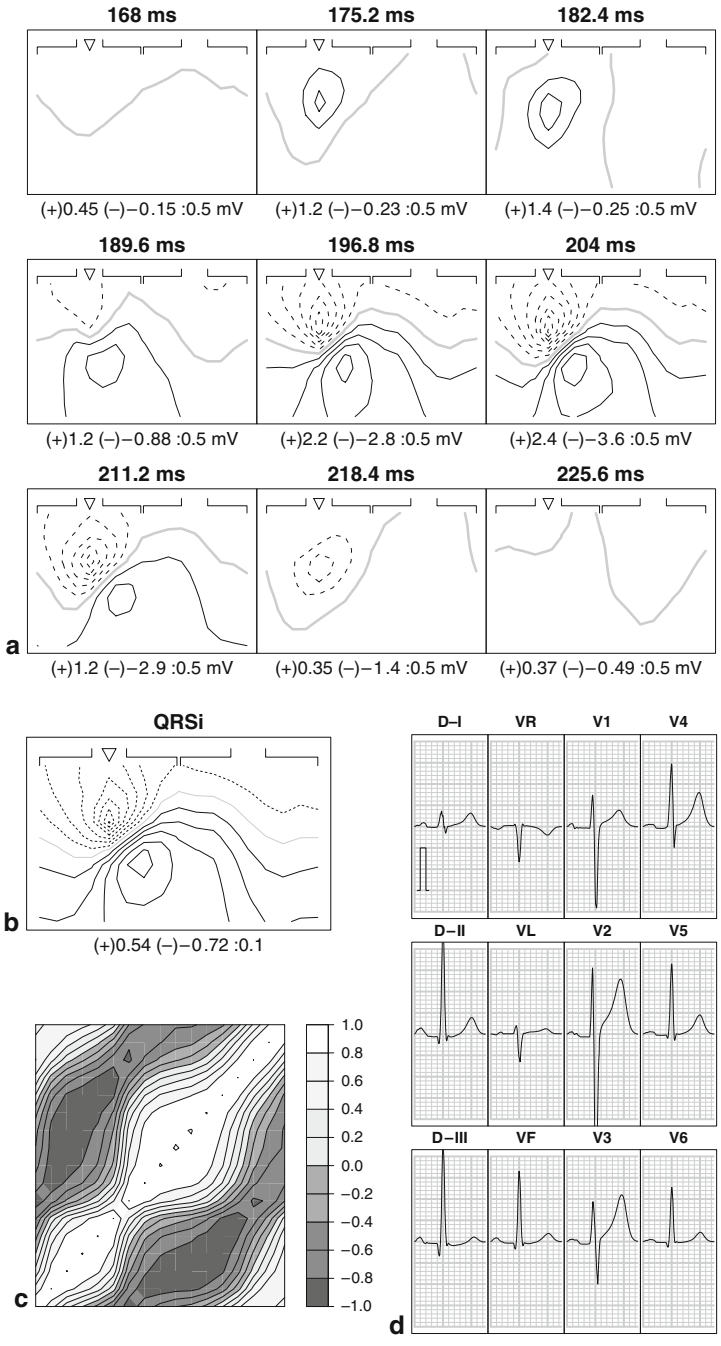

Figure 32.4

Different representations of depolarization potentials of the same cardiac cycle in a normal subject. (a) Successive, instantaneous potential maps during the QRS; conventions are as in Fig. 32.2, except that the lines are isopotential and are measured in mV; the label above each map indicates the timing of the instantaneous map. (b) Integral map with the same conventions as in Fig. 32.2. (c) Autocorrelation map of the QRS interval; the same time interval is on both *x*- and *y*-axis, and each point on the map represents the correlation coefficient between instantaneous potential distributions at the instants of its *x*- and *y*-coordinates, using shades of gray from black for −1.0 to white for 1.0, as indicated on the scale at right. (d) Standard ECG reconstructed from leads corresponding to the standard ECG leads, extracted from the body-surface lead system.

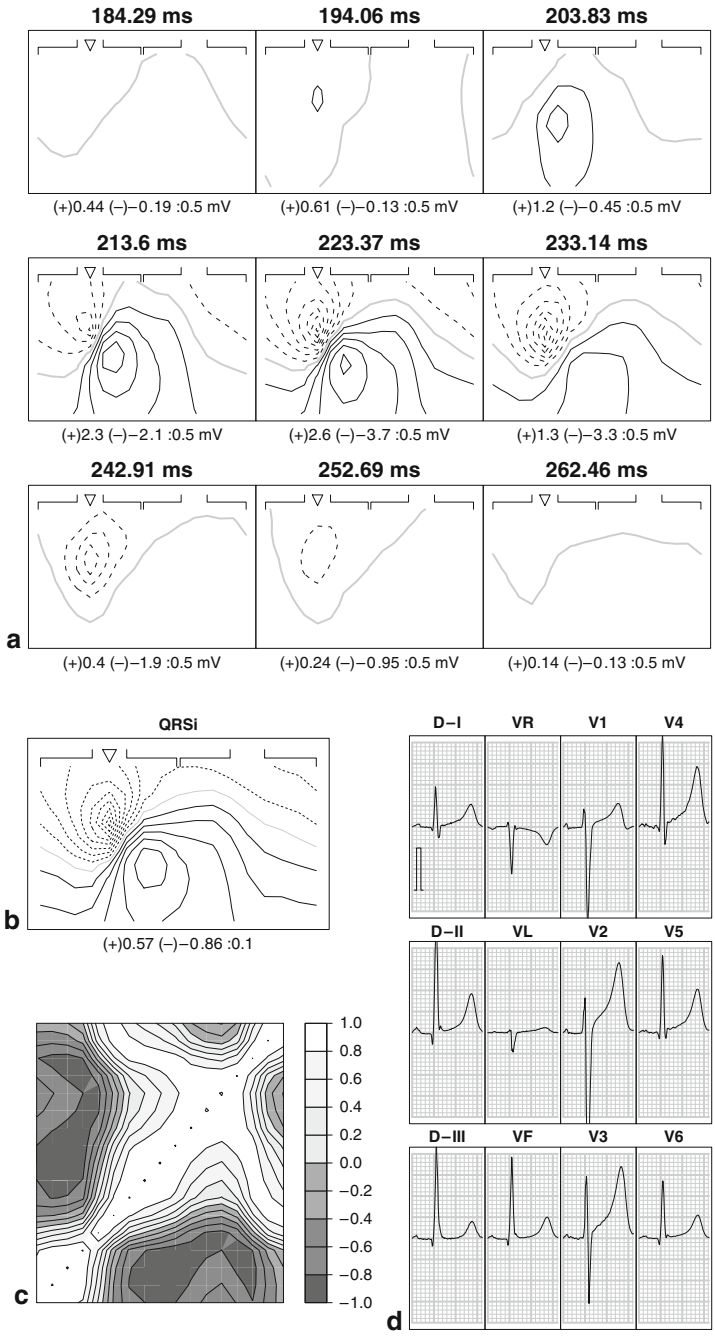

Figure 32.5

The same representations of ventricular activation as in Fig. 32.4, for one cardiac cycle in a different healthy individual. This recording was selected from a set of 236 in healthy people as a recording with an almost identical QRS integral as that in Fig. 32.4. Note the similarity of the 12-lead ECG, the visible differences in the instantaneous potentials and the striking differences in the AC map.

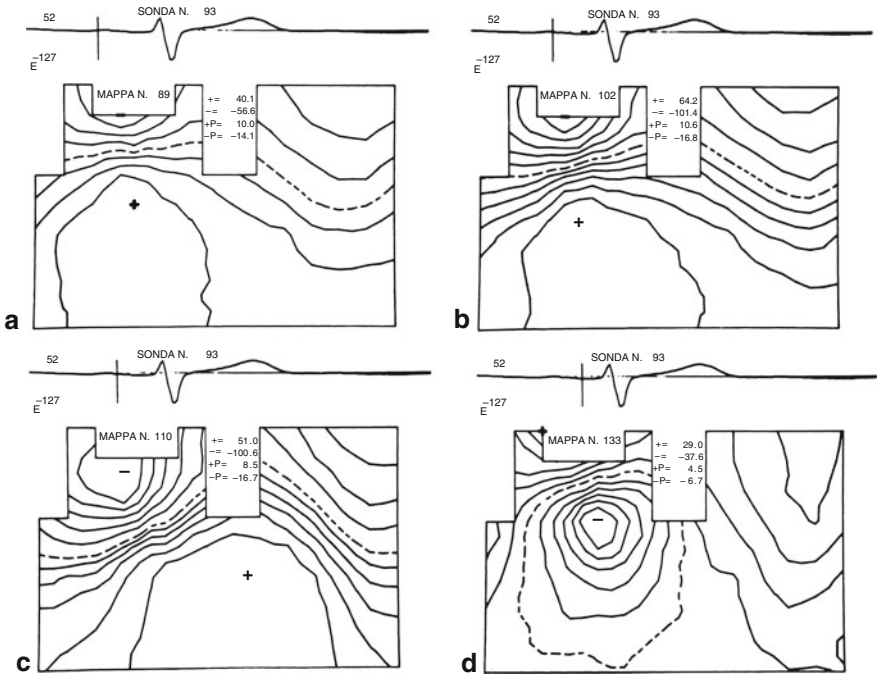

Figure 32.6

Averaged surface maps relating to atrial activation and recovery in a normal subject, at the instants or time indicated by the vertical line crossing the ECG at top of each figure. The time interval between the (a) and (d) is 88 ms. The zero equipotential line is dashed. The plus and minus signs indicate the value of the positive and negative peaks in microvolts; +P and −P indicate the step (in microvolts) between adjacent positive and negative equipotential lines.

32.4.2 Ventricular Activation

Body-surface potential distributions during ventricular excitation have been described by many investigators in adults [9, 19–21], children [22, 23], and infants [24, 25].

The main features of maps observed in adults are as follows. At the beginning of the QRS, a potential maximum appears in the upper or mid-sternal area, and a minimum is generally located in a lower position on the left thoracic wall or on the back (Fig. 32.7a). This potential pattern can be related to septal excitation, which occurs in a predominantly left-to-right direction [26, 27] and probably also to right ventricular free wall activation.

Later, the minimum migrates dorsally. In 25% of subjects, the migration is discontinuous: a separate low-amplitude dorsal minimum appears before the left lateral initial minimum has disappeared. Thus, in these subjects, two distinct minima are simultaneously present during the initial 15–20 ms of QRS [28]. The minimum then moves toward the right shoulder and finally appears in the right clavicular area (Fig. 32.7a, b). In some cases, the minimum moves horizontally around the back and reaches the right axillary region. This behavior has been observed particularly in subjects with left axis deviation in the standard 12-lead ECG. Meanwhile, the maximum migrates downward to the left mammary region (Fig. 32.7c). The events described above are temporally related to the spread of excitation in an endo-epicardial direction through the walls of both ventricles, with a mean direction from base to apex.

Thereafter, a new minimum often appears in the midsternal area (60% of cases in the authors' studies), at 14–44 ms after the onset of ventricular activation (Fig. 32.7d). This minimum is considered to be the surface manifestation of the right ventricular breakthrough, that is, of the presence of a "window" in the advancing wavefront, through which the currents reenter the heart. In the following instants, the sternal minimum and the right clavicular minimum merge to form a single, broad anterior negative area (Fig. 32.7e). In about 40% of the cases, the sternal minimum does not appear as a separate entity, and the sternal area becomes negative as a result of the migration of the main minimum.

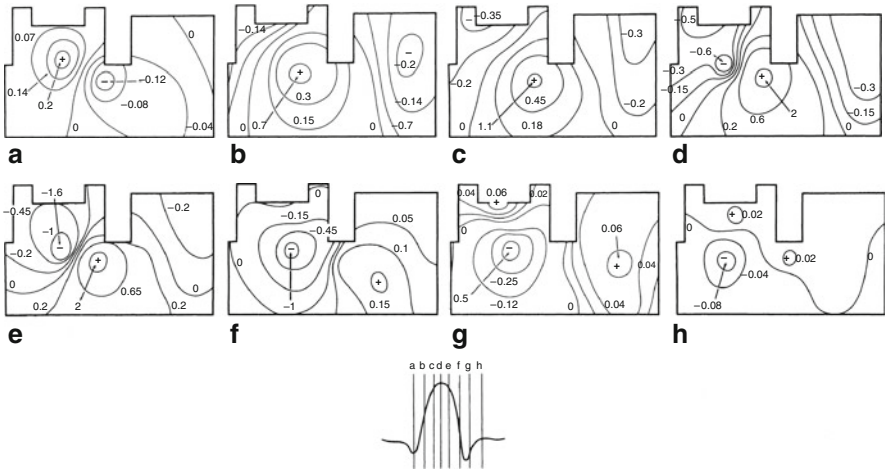

Figure 32.7

Body-surface potential maps during normal ventricular activation. Each map refers to the instant or time indicated by the vertical line crossing the ECG (*bottom*). The potential values are expressed in millivolts.

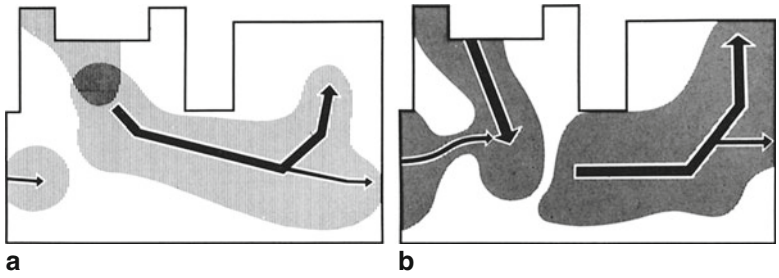

Figure 32.8

The shaded areas encompass all locations of the potential maxima (a) and minima (b) throughout the QRS interval in 50 normal subjects. The *arrows* indicate the main direction of migration of the principal maximum (a) and minimum (b). (After Taccardi et al. [15]. © Clarendon, Oxford. Reproduced with permission.)

Later, the maximum moves toward the left thoracic wall and then dorsally (Fig. 32.7f). In about 55% of adults, a new maximum appears in the upper sternal area during the last 20–30 ms of the QRS interval (Fig. 32.7g). In the great majority of cases, the second maximum appears while the dorsal maximum is still present, the time overlap being 10–30 ms. These potential patterns most likely indicate the presence of two separate excitation waves travelling through the heart. The dorsal maximum may be related to the activation of the posterobasal portions of the ventricles, and the upper sternal maximum to the excitation of the crista supraventricularis and pulmonary infundibulum. The time relationships between the two maxima may provide some indirect information about the time-course of excitation waves in the heart.

Green et al. [21] defined the range of normal body-surface potentials in a large population (1,113 subjects, aged 10–80 years) as a function of age, sex, and body habitus. On average, QRS potentials decreased with increasing age. Potential pattern distributions remained constant from 10 to 40 years; about 30% of the subjects older than 40 years had early negative potentials recorded more diffusely over the right thorax. This resulted in more vertically oriented zero equipotential lines. Only minor differences concerning QRS potential amplitude and distributions were noted when male and female subjects were compared within groups of similar age and body habitus.

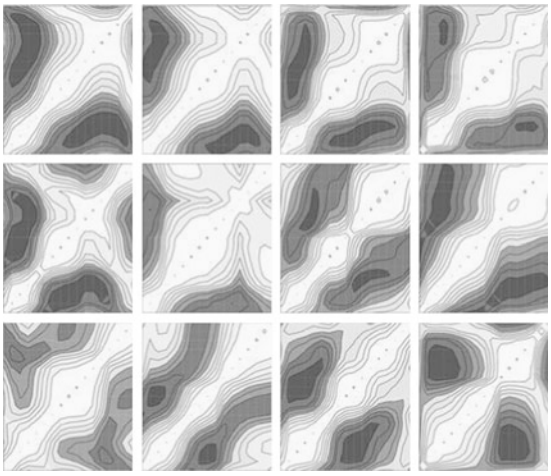

Figure 32.9

AC maps of body-surface recordings during the QRS interval in 12 healthy individuals, which are representative of the normal variability of ventricular depolarization. Same conventions as in Fig. 32.4c.

Interindividual variability is due to variability of the thorax conductor [29] and source variability [30]. Normal variability of the ventricular activation may be due to the well-known variability of the conduction system.

We computed AC maps in 236 normal recordings from the dataset of Dr. F. Kornreich (Vrije University of Brussels, Belgium). We sorted them using divisive clustering analysis taking the correlation coefficient as a measure of distance between AC maps. Twelve prototype cases spanning the whole spectrum of variability of AC maps of normal activation are shown in Fig. 32.9. In each activation AC map, the size of white ($R > 0.8$) regions along the main diagonal corresponds to periods of relative stability of body-surface distribution of potentials (apart from amplitude). Sometimes, these regions are distinct, as the transition from one pattern to the next is sudden (as in types 3 and 4), while in other cases, it is less distinct, as the transition is gradual (as in type 10). Usually, three such phases can be identified, the first two being separated by the ventricular breakthrough. The dark region, which occurs symmetrically between the first two phases, corresponds to the relatively opposed disposition of potential extrema on the body surface before and after ventricular breakthrough. The third phase corresponds to activation of the basal regions of the ventricles and pulmonary infundibulum and has a very variable relationship with the first two.

The amplitudes and surface distributions of time integrals during ventricular activation were firstly reported by Montague et al. [31] in 40 men and 15 healthy women and subsequently by many other authors. The QRS integral map is characterized by a dipolar distribution with a minimum in the mid-sternal area and a maximum in the left mammary-axillary region (Fig. 32.2).

In children, the main features of the maps are similar to those observed in adults. There are, however, minor differences; for instance, the sternal maximum during the last stage of QRS was present only in a small percentage of children [22], but invariably appeared during peak inspiration in the series of subjects studied by Flaherty [32]. According to Liebman et al. [23], the location of the terminal maximum can be right superior-anterior, anterior-superior, or right posterior, probably suggesting that the end of activation is in the right ventricular outflow tract, in the superior septum, or in the posterobasal left ventricle.

In newborn infants, Tazawa and Yoshimoto [24] observed that during ventricular excitation, the initial potential maximum migrated to the right instead of moving to the left and dorsally as in normal adults. This behavior of the maximum was attributed to the physiological predominance of the right ventricle in the newborn heart. Benson et al. [25] described the evolution of the surface potential during ventricular excitation and recovery in the first year of life. There was a progression of change in the body-surface QRS potential distribution: at birth. A single QRS maximum migrated to the right during the second half of QRS; at several months of age, the initial maximum evolved into two maxima: one moving to the right, and the other to the left; at 9–12 months of age, the initial maximum moved to the left lateral

thorax, while the right maximum almost disappeared. Moreover, the age-related changes of the QRS maps were associated with similar changes on the repolarization maps; with increasing age, movement of both the excitation and the recovery positive potentials to the right chest progressively disappeared.

32.4.3 Ventricular Repolarization

Sizeable recovery potentials usually appear at the surface of the body before the end of the QRS interval [14] (Fig. 32.7h). This finding was confirmed and quantified by Spach et al. [33], who also reported that the time overlapping of excitation and recovery potentials varied in different age groups, being greater in younger classes (8–12 and 20–29 years). In some subjects, the overlap lasted for 12–28 ms. The first signs of repolarization consist of a potential maximum, which generally appears on the sternal area, on the left precordium or, in a few cases, even more laterally, on the left axillary region (Fig. 32.7h). In the latter case, the maximum soon moves toward the central anterior chest area (Fig. 32.10a). During the early phase of recovery, the minimum is often ill-defined. The most negative areas can be found anywhere around the maximum, in the anterior lower part of the torso, in the lateral wall, or in the back [14].

This potential distribution is essentially in agreement with that described by Spach [33] in subjects 8–60 years old during the first 50 ms of ventricular recovery. Within 100–150 ms from the onset of ST the most negative potentials concentrate in an area covering the right scapular region, the right shoulder, the clavicular, and the upper sternal regions (Fig. 32.10). In a minority of adult subjects, the most negative areas are located in the right clavicular or scapular regions from the beginning of repolarization. During the T wave the minimum is consistently found in the right clavicular or scapular areas and the maximum in the precordial region [12, 14]. Slight shifts of the potential extrema are usually observed during the entire T interval (Fig. 32.10).

In a large normal population, Green et al. [21] observed that ST-T potentials decreased with age in both sexes. Moreover, in female subjects over the age of 40, there were more extensive low-level negative potentials over the precordium during the ST segment than in men. On the other hand, male subjects consistently showed greater T potential amplitudes.

The early repolarization deviation index (ERDI, see Sect. 32.3.4) is about twice as high as in females compared to males [34]. LRDI is higher in males. As the correlation coefficients between instantaneous potentials in the same subject are invariant to the features of the thorax conductor [13], it proves that gender differences in repolarization potentials are not entirely due to the systematic anatomical differences in thorax shape and conductivity between the genders, but must be due, at least in part, to differences in myocardial repolarization gradients.

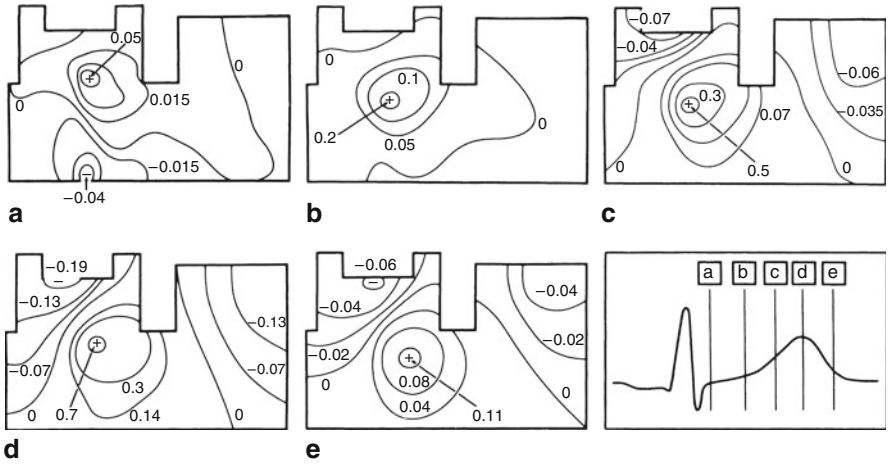

Figure 32.10

Body-surface maps during normal ventricular recovery. Each map refers to the instant or time indicated by the vertical line intersecting the ECG. (After Taccardi et al. [15]. © Clarendon, Oxford. Reproduced with permission.)

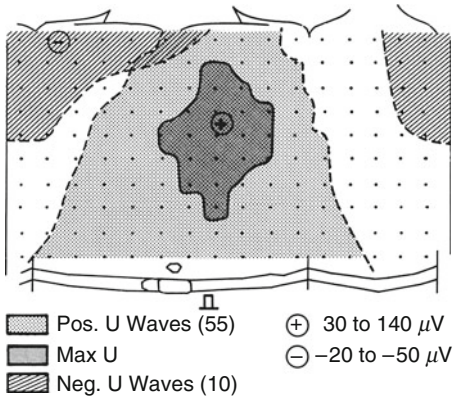

Figure 32.11

Location or potential maxima and minima during the U wave in 55 normal subjects aged 8–60 years. (After Spach et al. [17]. © American Heart Association, Dallas, Texas. Reproduced with permission.)

The integral maps of QRST deflections are thought to provide valuable information on the ventricular recovery process [35]. Areas of QRST deflection mainly reflect the intrinsic recovery properties and are largely independent of the ventricular excitation sequence. Actually, at the body surface, negative QRST integrals should be recorded from areas facing myocardial regions with longer recovery durations, whereas positive values are recorded from the thoracic surface facing cardiac regions with shorter recovery durations.

In normal subjects the ST-T and the QRST integral maps show a bipolar distribution of the values with a minimum on the right clavicular–upper sternal areas and a maximum on the mammary region (Fig. 32.2).

A few descriptions of accurate recordings of potential distributions during the U wave have been reported [17, 36, 37]. Spach and associates [17] studied 11 children aged 1–7 years and 55 subjects aged 8–60. In the 11 children, no measurable U wave was found. In the remaining subjects, positive U-wave potentials were located within a broad area on the anterior and left lateral chest surface (Fig. 32.11); the magnitude of the potential maximum varied from 30 to 140 μV. The highest U voltages were confined to the precordial area where the highest T voltages occurred. In most subjects, the specific locations of T-wave and U-wave maxima were coincident; in 17 subjects, the U-wave maximum was slightly to the right of the T-wave maximum. Clear-cut negative U waves were found in only 10 of the 55 subjects. The negative peaks varied from −20 to −50 μV and occurred on the right clavicular or scapular areas (Fig. 32.11).

32.5 BSPM in Heart Disease

32.5.1 Ischemic Heart Disease

32.5.1.1 Myocardial Infarction

Descriptions of the potential distribution on the body surface in patients with anterior or inferior myocardial infarction (MI) have been published by many authors [38–53].

An attempt was made to define quantitatively the characteristic features and the range of variation of surface maps in anterior and inferior myocardial infarction during ventricular activation and recovery [38].

In patients with anterior MI (Fig. 32.12), at the onset of ventricular activation, the potential minimum was located in the sternal or left mammary region. In some patients, the minimum lay outside the area where the minima were located in normal subjects. In MI patients, the minimum remained confined to a limited zone on the anterior chest wall throughout the QRS interval, whereas in normal subjects, it migrated leftward and dorsally.

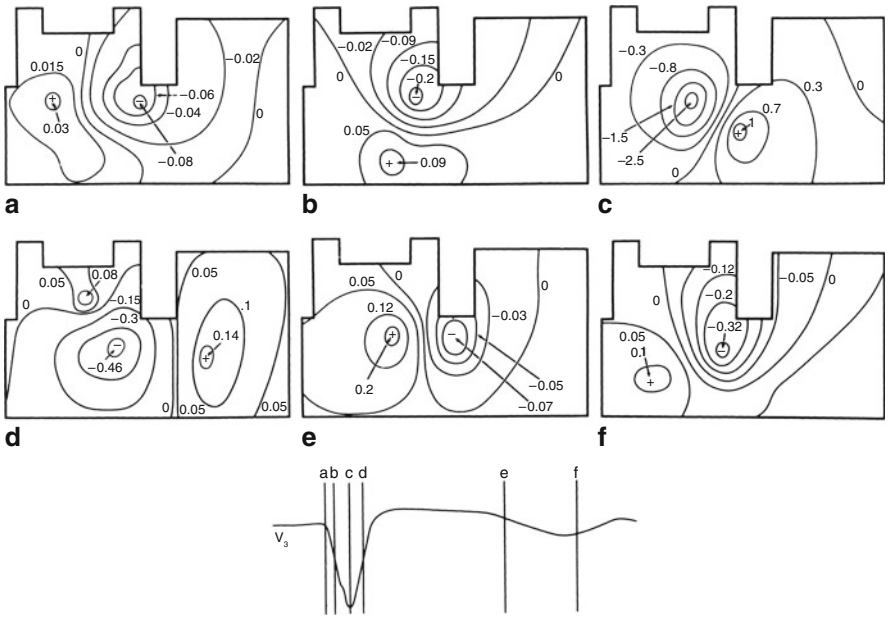

Figure 32.12

Body-surface maps in a subject with anterior MI. Each map refers to the instant of time indicated by the vertical fine crossing the ECG. Potential values are expressed in millivolts.

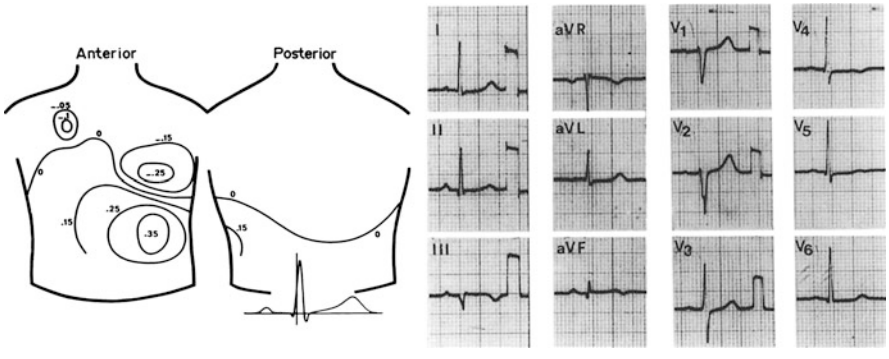

Figure 32.13

Body-surface map of a patient with an old anterior MI not revealed by the 12-lead ECG. During the early phases of the QRS interval an abnormal potential minimum is present on the left mammary region above the area explored by the standard precordial leads.

The persistence of a negative area on the anterior chest surface could be ascribed to the presence of an infarcted region in the underlying ventricular wall. This region did not depolarize and thus acted as a current sink. Occasionally, the minimum was located above the area explored by conventional precordial leads; in these cases, as in Fig. 32.13, the l2-lead ECG did not reveal any sign of anterior MI although there are suspicious changes in the inferior leads III, aVF, and the anterolateral leads V4–V6. In 13 subjects with anterior MI, the highest absolute value of the potential minimum varied between 1.06 and 4.77 mV (mean 2.78 ± 0.3) and was significantly higher than in normal subjects ($p < 0.01$).

At the onset of ventricular activation, the location of the potential maximum was normal in the majority of cases. However, the migration of the maximum was clearly abnormal, as could be expected since the area through which the maximum should normally have passed during its migration was occupied by the potential minimum. During the first 30 ms of ventricular activation the behavior of the maximum varied. In the majority of cases, it moved superiorly toward the neck, then posteriorly toward the left scapular region, and finally reached the left axillary region; in other patients (Fig. 32.12), the maximum migrated inferiorly on the anterior chest wall and reached the left axillary region; in two cases, in which the maximum was located in the left submammary region, it stayed in the same area. These various trajectories were probably related to the different extent and topography of the infarction. During the following phases of ventricular excitation the behavior of the potential maximum was within normal limits. The highest value reached by the potential maximum was significantly lower than that observed in normal subjects (mean 1.29 mV ± 0.23 standard error; $p < 0.01$). Moreover, the highest positive value was reached later than in normal subjects ($p < 0.01$), occurring between 30 and 66 ms (mean 41.8 ± 2.6).

At the beginning of the ST interval, the surface potential values were very low and the potential minimum was ill-defined, whereas the maximum was usually well developed, as occurs in normal subjects. The electronegative areas were located either on the left lateral wall of the chest, or on the lower part of the back, or both. These features are similar to those observed in normals. During the T interval, a clear-cut minimum generally appeared in the left mammary or submammary region. This location is definitely abnormal (see Fig. 32.10). In some patients, another minimum was simultaneously present in a normal area; that is, the upper sternal region. The location of the T minimum over the precordial area facing the infarction could be explained by assuming that the infarcted area did not generate recovery currents of its own and acted as a sink for repolarization currents originating in the surrounding, uninjured myocardial tissues. The highest values reached by the recovery maximum were significantly lower than in normal subjects ($p < 0.01$), whereas the highest values reached by the minimum were significantly higher ($p < 0.01$).

During the ST interval and the initial portion of the T wave, the recovery maximum was located within the normal area on the anterior chest wall (Fig. 32.12e). During the second half of the T wave, in the majority of cases, the potential maxima moved away from the area where they had appeared (Fig. 32.12f), and mainly scattered over the anterior lower thoracic surface. This late migration of the potential maximum was not observed in any of the normal subjects. This phenomenon is quantified by the late repolarization deviation index (LRDI, see Sect. 32.3.4), which increases in non-ischemic ventricular hypertrophy [54] as well as in old myocardial infarction compared to normal [55], even when adjusted for gender, being higher in males [34].

In the 14 cases of inferior myocardial infarction (Fig. 32.14), the potential minimum was located within or near the normal area at the beginning of the QRS interval. It then moved to the inferior half of the posterior or anterior chest wall, thus passing beyond the limits of the normal scatter for the relevant instants of time. At 20 ms, the minimum was located outside the normal area in the great majority of patients. The low position of the minimum, which was observed in all patients with inferior MI at 20–30 ms, was most likely related to the presence of an infarcted area in the diaphragmatic wall of the heart. This area of non-depolarizing tissue acted as a "window" through which the depolarization currents generated by normal cardiac muscle reentered the heart.

During the following instants, the minimum migrated toward the midsternal region in some patients; in the other patients (Fig. 32.14b), a new separate minimum appeared in the sternal region between 22 and 42 ms after the beginning of the QRS interval, while the first minimum was disappearing. Here, as in normal subjects, the sternal minimum was attributed to right ventricular breakthrough.

The highest absolute value of the negative potential varied between 0.45 and 1.67 mV (mean 1.3 ± 0.1) and was significantly lower than in the authors' normal subjects ($p < 0.01$). The low absolute value reached by the sternal minimum could be explained by the fact that the solid angle viewing the negative aspect of the wavefront from the sternum was smaller than in normal conditions because the wavefront did not extend over the entire diaphragmatic wall of the heart. In the authors' experience, in patients with inferior myocardial infarction, the behavior of the potential maximum during the QRS interval (Fig. 32.14), its area of distribution, and its highest absolute value were within normal limits.

At the beginning of the ST interval, electronegative areas could be found on the lower half of the trunk anteriorly and posteriorly, as in normal subjects. During the T wave, the recovery minimum moved to or remained in the inferior half of the trunk (Fig. 32.14e). The abnormally low location of the minimum during the T wave could be ascribed to the presence of an infarcted area in the diaphragmatic wall of the heart, which acted as a sink for recovery currents.

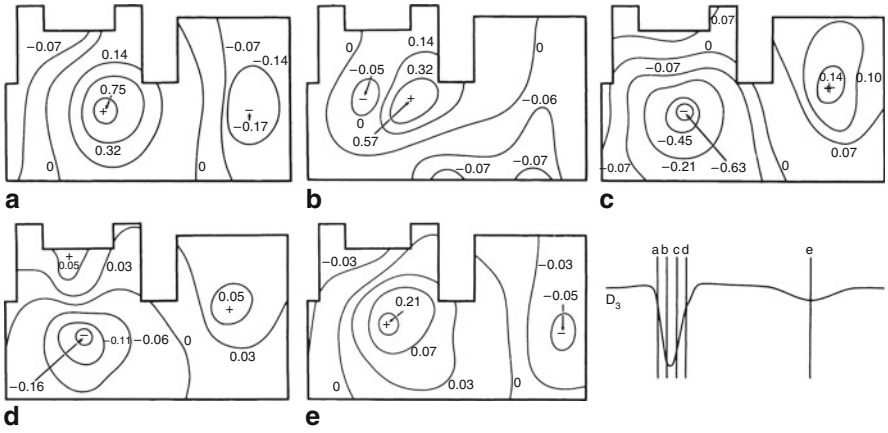

Figure 32.14

Body-surface map of a patient with inferior MI. Each map refers to the instant of time indicated by the vertical line crossing the ECG. Potential values are expressed in millivolts. The time interval between successive bars is 15 ms.

The location of the recovery maximum was within the normal area, i.e., the sternal or left mammary region, during the entire recovery process (Fig. 32.14e). The highest absolute values reached by the recovery maximum and minimum were not significantly different from those observed in normal subjects.

Potential patterns similar to those mentioned above were also described by Vincent and coworkers [43] in 28 subjects with inferior MI. These authors were also able to detect on BSPMs the characteristic features of inferior infarction in eight patients, whose ECGs had returned to normal or were nondiagnostic for the previous infarction. Similar findings were obtained by Osugi et al. [47].

Hirai et al. [48] described an abnormal location of the minimum at 15 ms into the QRS in 26 of the 32 cases of anterior myocardial infarction with a normal 12-lead ECG.

The possibility of detecting signs of myocardial infarction by means of body-surface mapping, even when the conventional ECG was within normal limits, was also demonstrated by Flowers et al. [41, 42]. Using departure maps, abnormalities of potential distribution were found in patients with anterior or inferior MI at the onset of ventricular excitation (corresponding to the Q wave in the conventional ECG) and during the mid-phases and late phases of the QRS interval [41].

Ohta et al. [46] compared body-surface maps with left ventriculographic findings in 24 patients with old inferoposterior MI. Using the departure-map technique as proposed by Flowers [41], they found surface potential abnormalities owing to infarction during specific phases of the QRS interval and in specific areas on the chest surface, depending on the location and extent of ventricular asynergy. In particular, some patients with inferior MI and, in addition, severe asynergy of the anterior, apical, or septal segments but without ECG or VCG signs of anterior MI, exhibited definite abnormalities of departure maps, which were different from those related to purely inferior MI.

De Ambroggi et al. [39] recorded BSPMs in 30 patients with old inferior myocardial infarction. Of these, 15 had no signs of necrosis in the conventional ECG. A number of variables relative to the instantaneous potential distribution and to integral maps were considered. The most accurate diagnostic criterion was derived from the integral values of the first 40 ms of QRS, with a sensitivity of 73% in patients without signs of necrosis in the 12-lead ECG, and of 100% in patients with pathological Q waves in the ECG, with a specificity of 83%.

In non-Q myocardial infarction of the anterolateral wall, the integral maps of the first 40 ms of QRS provided a good sensitivity (67%) in detecting signs (areas of values two standard deviations lower than normal) of the old necrosis in a group of patients with normal ECG [40].

Medvegy et al. recorded BSPM in 45 patients with documented non-Q-wave MI [52]. The main abnormality revealed by BSPM was the loss of electrical potential, but different features were characteristic for each region of the heart, so that they were suitable for the detection and localization of non-Q-wave MI, in the clinical setting of unstable coronary artery disease.

32.5.1.2 Acute Myocardial Infarction

Since the late 1970s, a simplified method of electrocardiographic mapping has been widely used in acute MI in order to obtain data on the infarct size and to assess the efficacy of various therapeutic interventions aimed at limiting myocardial injury [56].

The simplified method consists in recording 35–70 ECGs from the left hemithorax and in calculating the sum of the amplitudes of ST-segment elevations at all electrode sites, and the number of points with ST elevation. Similar procedures have also been used to evaluate the appearance of pathological Q waves and the reduction of R waves on the thoracic area explored.

The use of thoracic maps for assessing infarct size is based on experimental observations in animals demonstrating that any intervention that provokes an extension or reduction of the epicardial ischemic areas produces similar variations of the precordial areas, in which ST elevation is recorded [57, 58]. The use of these simplified methods of electrocardiographic mapping for assessing the extent of the infarction has aroused much criticism [59, 60]. In fact, there are several factors, other than the dimensions of the infarct, which can influence the ST segment elevation and, to a lesser extent, the QRS complex. These factors consist of local intraventricular conduction disturbances, electrophysiological changes in the myocardium outside the ischemic area, electrical cancellation phenomena, intra-extracellular electrolyte levels, pericarditis, heart rate, and autonomic nervous system activity. Despite the above considerations, the method does offer some definite advantages in monitoring patients with acute MI, in that it can reveal variations in the extent and severity of the ischemic process earlier than other methods, such as enzyme levels and myocardial scanning.

A description of the ST-T potential distribution on the entire chest surface in acute MI was reported by Mirvis [61], who observed a characteristic early appearance of the repolarization potentials in both anterior and inferior MI, with a longer than normal overlap between final excitation and recovery potential patterns. During the ST-T interval, the potential distributions were characterized in anterior MI by a single maximum on the left anterior chest that remained fixed in location but increased in amplitude as repolarization progressed; in inferior MI, there was a single minimum generally located on the left anterior-superior thorax, with positive potentials covering the lower thoracic portions.

The distribution of QRS and ST potentials in acute inferior myocardial infarction (mean 76 h after the onset of symptoms) has been studied by Montague et al. [62]. They computed integral maps in a group of 36 patients with acute inferior MI, and found negative areas over much of the inferior torso with extension of the positivity to the superior torso, during the first half of the QRS interval (Q zone); conversely, the ST segment integral map was characterized by abnormally positive inferior distributions and concomitant negative precordial distributions. Moreover, patients with right ventricular involvement tended to have a greater area of negative Q zone over the right anterior inferior thorax and greater inferior and rightward extension of ST segment positivity as compared with patients with exclusive left ventricular infarction. Thus, in acute inferior MI, BSPMs make it possible to detect definite abnormalities of both depolarization and repolarization potentials, which indicate right ventricular involvement.

More recently, Menown et al. [63] confirmed the ability of BSPMs (using 80 leads) to improve, with respect to conventional ECG, the classification of inferior acute MI with posterior or right ventricular wall involvement.

The same group demonstrated that the BSPM diagnostic algorithm detected acute MI with higher sensitivity than a 12-lead ECG diagnostic algorithm or a physician's interpretation, without loss of specificity [64]. They also showed the superiority of BSPM versus the 12-lead ECG in detecting acute MI in the presence of left bundle branch block (LBBB) [65].

32.5.1.3 Myocardial Ischemia

In angina patients, the resting ECG is very often normal between attacks. This can indicate that cardiac electrogenesis is normal or that there are electrical abnormalities, which are not revealed by the conventional ECG because they are too small, or because they are projected to surface areas not explored by conventional leads.

In several patients with proven angina pectoris and a normal resting ECG, surface maps exhibited an abnormal distribution of recovery potentials [66]. In these patients, the location of the potential minimum during recovery was outside the normal range during some phases of the ST segment and of the T wave, often on the lower left lateral region of the chest (Fig. 32.15a).

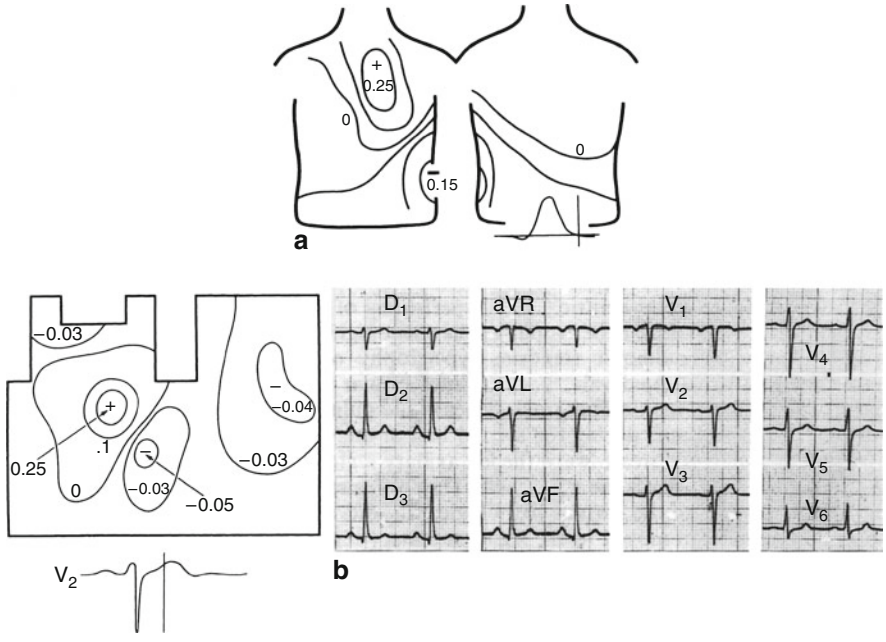

Figure 32.15

(a) BSPM of a patient with angina and normal resting ECG. The map refers to the early ST interval, as indicated by the vertical line crossing the ECG. This potential pattern lasted about 200 ms. Potential values are expressed in millivolts. (b) BSPM at the instant indicated by the vertical line crossing the ECG, in a patient with angina but normal T waves on the resting ECG. The map shows a complex potential distribution with one maximum and two minima.

During the entire ST-T interval the potential maximum was located within the normal area in most patients with angina. Only in a few subjects was the location of the maximum abnormal during the final phases of ventricular recovery. In some of these patients with angina and a normal resting ECG, a complex potential distribution was observed (Fig. 32.15b), with one maximum and one minimum located normally and a second minimum placed in an abnormal position.

In a study [67] performed on 14 patients with stable angina and a normal resting ECG, the analysis of BSPMs was extended to a new series of quantitative aspects; that is, temporal evolution during the ST-T interval of the highest potential on the chest, lowest potential, highest potential difference, integral of the absolute value of the potential function extended over the entire chest surface, and the percentage of the total thoracic area with positive potentials. By deriving a number of voltage-related variables from these time functions and by submitting them to multivariate analysis, it was possible to separate more than 90% of the ischemic patients from normal subjects. It has been shown [68] that, in some patients with typical angina but no evidence of MI, QRS potentials can differ from normal at some chest locations, which are not explored by the standard 12 leads.

BSPMs were also used to study the potential variations before, during, and after coronary angioplasty (PTCA). During balloon inflation in the anterior descending or right coronary artery, specific changes of QRS instantaneous and integral maps were observed, suggesting a regional conduction delay due to myocardial ischemia [69].

Shenasa et al. [70] demonstrated potential patterns 40 ms after QRS end during inflation that were specific to the three major coronary arteries dilated. The left anterior descending coronary artery was associated with the largest ST-segment shifts with a precordial maximum and negative potentials over the back; for the right coronary artery, negative potentials covered the upper left torso with a left mid-axillary minimum and positive potentials over the rest of the torso; for the left circumflex coronary artery, negative potentials covered the anterior torso with a precordial minimum and positive potentials over the back. These changes disappeared rapidly after balloon deflation. Thus, BSPMs provide a comprehensive

approach for the evaluation of electrocardiographic changes and the development of optimal leads for the detection of acute occlusion of a coronary artery.

BSPMs were also used to evaluate the clinical efficacy of PTCA and were proved useful to detect restenosis [71].

32.5.1.4 Exercise Maps

Potential maps have been obtained during exercise in normal subjects and patients with angina.

Some authors [72] recorded ECGs from 16 points located on the left anterior thorax, using traditional methods. This technique should be more appropriately considered as a system of multiple precordial leads rather than surface mapping. The 16-lead system, however, has shown greater sensitivity than 12 standard leads or three orthogonal leads [73], although this has not been confirmed by other groups.

Other investigators studied the instantaneous potential distribution on the anterior thorax [74, 75] or on the entire chest [76–79]. A complete and accurate study on the QRS and ST-T wave changes induced by exercise was performed by Spach's group in healthy subjects [76]. These authors were able to obtain high-quality potential maps during exercise without averaging ECG waveforms, by using their system for calculating total body potential distributions from 24 chest leads. Exercise induced consistent changes in potential patterns. During the first 20 ms of QRS, the minimum stayed on the lower left chest, while, in the resting condition, it gradually migrated toward the upper back. In mid-QRS, the magnitude of the anterior potential maximum was approximately 60% of that observed in the map at rest while the duration of the QRS interval usually increased (2–10 ms) at peak exercise. On the basis of these findings, it was suggested that the decrease in the magnitude of the precordial potential maximum in the midportion of QRS (R wave in lead V5) might result from changes in the sequence of activation of the ventricles, rather than from blood volume variations (Brody effect).

In the early stage of ventricular repolarization (early ST segment), a potential minimum usually developed on the lower left thorax during exercise. This minimum generally decreased in magnitude in a short time after exercise. During the subsequent instants of the ST interval, the lower left precordial region became less negative and was usually positive by the early portion of the T wave. At the peak of the T wave the potential pattern showed slight changes during and after exercise with respect to the resting condition. However, the amplitude did change considerably. In particular, immediately after exercise, the magnitude of T-wave potentials increased rapidly, reaching its highest value 30–90 s after the end of exercise, before gradually decreasing; in some subjects, the potential values were still higher than resting values 10 min after exercise.

In patients with angina, Simoons and Block [77] reported some typical changes induced by exercise. The recovery minimum was located in the lower part of the left side of the chest and attained −90 μV or more 60 ms after the end of the QRS complex. This repolarization pattern was found in 21 out of 25 coronary patients, but in none of the normal subjects (sensitivity 84%, specificity 100%).

Yanowitz et al. [79] recorded BSMs before and after exercise in 25 males with documented coronary disease. By considering the integrals of the first 80 ms of the ST interval, they found abnormal negative values in 18 cases. Moreover, in 25% of the cases, BSPMs after exercise showed maximal depression of the ST-segment area at sites not sampled by the leads usually employed in exercise testing. This finding suggests that BSPMs may increase the sensitivity of the exercise testing for coronary disease.

32.5.2 Right Ventricular Hypertrophy

Hypertrophy may involve various portions of the right ventricle in different forms of heart disease. In children BSPMs were recorded in the following types of right ventricular hypertrophy (RVH) [80]: dilation of right ventricle and hypertrophy of the crista supraventricularis owing to secundum atrial septal defect; hypertrophy of the entire right ventricle, including the outflow tract, secondary to valvular pulmonic stenosis; hypertrophy of the proximal portion of the right ventricle between the tricuspid valve and the infundibular stenosis, with normal thickness of the right ventricular wall in the outflow tract, beneath the pulmonary valve (tetralogy of Fallot).

While, in normal subjects, during the second half of the QRS interval, the potential maximum moves from the precordial area toward the left axillary region and then to the back, in all patients with RVH, it migrated toward the right chest.

The movement of the maximum on the right thorax was different according to the various pathological conditions [80]. In atrial septal defect (ostium secundum) the maximum moved to the right mammary region, finally reaching the upper sternal region. In tetralogy of Fallot with infundibular stenosis, the maxima migrated toward the right lateral thoracic wall. In valvular pulmonic stenosis, the maximum migrated on the anterior right chest toward the upper central area, as in atrial septal defect; the potential values, however, were markedly higher.

These surface potential patterns were correlated with the spread of excitation through the right ventricular wall, as determined in the same patients at surgery. In all three types of RVH, the activation wavefront moved on the epicardial surface in a rightward direction. In atrial septal defect, the latest epicardial events were recorded along the atrioventricular groove and gave rise to a right-chest maximum. However, after completion of epicardial excitation on the right ventricle, a potential maximum persisted over the upper sternal area. This terminal maximum was probably related to an activation wavefront spreading through the upper part of the septum and the crista supraventricularis, which is most likely hypertrophied in right ventricular volume overload.

In valvular pulmonic stenosis, as the wavefront moved laterally across the right ventricular free wall, it produced a maximum over the right chest while a minimum was positioned over the left precordium. The terminal excitation wavefront spread superiorly through the outflow tract of the right ventricle and gave rise to the upper sternal maximum.

In tetralogy of Fallot, after right ventricular breakthrough occurred, the wavefront moved laterally toward the atrioventricular groove and produced a maximum over the lower mid-right chest with a minimum in the left precordial region. The latest portions of the right ventricle to be depolarized were along the lateral inferior part of the atrioventricular groove. The final orientation of the wavefront was such that it resulted in a maximum in the right axillary region with a minimum over the central chest. Thus, maps enable the different types of RVH to be recognized to a greater extent than does the 12-lead ECG.

Body-surface maps in adult patients with RVH owing to mild-to-moderate valvular pulmonic stenosis were obtained by Sohi et al. [81]. Using departure maps, they observed a delayed appearance of the sternal negativity, which is usually related to right ventricular breakthrough, and an abnormal positivity located in the upper anterior chest.

32.5.3 Left Ventricular Hypertrophy

Body-surface maps in patients with left ventricular hypertrophy (LVH) owing to mild-to-moderate aortic stenosis were studied by Sohi et al. [81], using the departure-map technique. They observed an abnormal delay of early negativity on the anterior right chest and a potential maximum on the upper anterior chest, which peaked later and lasted longer than normal.

An assessment of left ventricular mass in patients with LVH was attempted by Holt et al. [82] on the basis of chest-surface potential distribution. They used a mathematical model in which the ventricles and the septum were represented by 12 dipoles. The dipole activity was assumed to be proportional to the amount of viable myocardium in that region; the strength of each dipole as a function of time was determined by measuring potentials at 126 locations on the thoracic surface and by applying suitable transfer coefficients. A good correlation was found between left ventricular mass determined by angiography and that determined by surface potentials ($r = 0.85$). Moreover, the correlation coefficient was much higher using BSMs than other electrocardiographic recordings (12 standard ECG leads or VCG).

Yamaki et al. [83] used BSPMs recorded with 87 leads to determine the severity of LVH in 57 patients with concentric hypertrophy and in 30 with left ventricular dilatation. A number of parameters related to QRS voltages and ventricular activation time were measured, and some of them were proven useful in determining the severity of LVH.

Kornreich et al. [84] studied BSPMs during the entire cardiac cycle (PQRST) in 122 patients with LVH. Best classification results were achieved with ST-T features, followed by features from the P wave, QRS, and PR segment. Cumulative use of ST-T and P features yielded a specificity of 94% with a sensitivity of 88%.

Hirai et al. [85] studied QRST integral maps in patients with LVH (10 with aortic stenosis, 12 with aortic regurgitation, and 22 with hypertrophic cardiomyopathy). Abnormalities in patients with hypertrophic cardiomyopathy were manifest even in mild LVH and a greater disparity of repolarization was found in hypertrophic cardiomyopathy than in LVH due to aortic valve disease.

We reported the results on BSPMs recorded in 16 patients with LVH due to aortic stenosis, focusing on the analysis of ventricular repolarization, with the aim of searching for subtle alterations not revealed by the usual ECG processing, which are likely to reflect ventricular repolarization heterogeneities [54].

The classical signs of LVH in the standard ECG (increased QRS voltage and ST-T changes) are reflected on BSPMs as (1) increased amplitude of the QRS integral map and of the STT integral map, (2) relatively low amplitude of the QRST integral map, due to the cancellation between the depolarization and repolarization potentials, and (3) opposing aspects of the QRS and STT integral maps.

In order to detect possible minor electrical disparities of repolarization not apparent from visual inspection of the ST-T and QRST maps, we analyzed the morphology of all the recorded ST-T waves, using principal component analysis. In our patients, the "similarity index," defined as the first eigenvalue divided by the sum of all eigenvalues, was slightly but significantly lower than in control subjects (0.73 vs 0.77; $p = 0.027$), suggesting the presence of a degree of heterogeneity of repolarization higher than in the normals. The repolarization deviation indices were also computed, as described in the methods. In our LVH patients, the changes during early repolarization, as reflected by ERDI, were similar to those observed in our control group and also in the larger group of 159 normal subjects from the database of Dr. F. Kornreich (Vrije University of Brussels, Belgium). Then, we focused on the analysis of the T peak-T end period, during which possible heterogeneities of repolarization should be more likely to be detected. The LRDI was significantly higher ($p = 0.005$) in LVH patients than in normals. The values of similarity index and LRDI found in LVH patients suggest a higher than normal degree of repolarization heterogeneity, not detected by the usual electrocardiographic analysis.

32.5.4 Right Bundle Branch Block

Several types of potential patterns have been observed in patients with right bundle branch block (RBBB) [86–88]. During the initial phases of ventricular activation, the surface potential distribution was similar to that observed in normal subjects with a maximum located on the sternal or left mammary region and a minimum on the left chest wall or in the dorsal regions (Fig. 32.16b). The sternal minimum, which indicates right ventricular breakthrough and which occurs in normal subjects 14–44 ms after the onset of the QRS complex, did not appear. Only at a later stage (38–70 ms after the onset of ventricular activation) did a second minimum appear, which, however, was located in an abnormal position, that is, in the left mammary region (Fig. 32.16d). It should be noted that this second minimum usually occurred to the right of the potential maximum located on the left precordium. This maximum was attributed to the spread of excitation through the left ventricular wall, while the delayed minimum was interpreted as the result of excitation arriving on the surface of the left ventricle, most probably in the left paraseptal region or in the apical area.

Shortly after the appearance of the second minimum, a new potential maximum appeared on the right precordium (Fig. 32.16c). This led to a complex potential distribution with two maxima (left and right) and two minima (on the right clavicular region and on the left precordial area), indicating the simultaneous presence of two excitation waves spreading into the left and right ventricles. Subsequently, the two negative areas merged, while the left maximum shifted to the back (Fig. 32.16g) and eventually disappeared, as in normal subjects, about 80 ms after the onset of the QRS complex. Thus, during the final stages of the QRS interval, only the signs of delayed right ventricular activation persisted, with a maximum on the right anterior chest wall and a minimum on the left precordial area (Fig. 32.17a–c). At the end of the QRS complex, early recovery potentials could often be observed before the last excitation potentials disappeared. Usually, the activation maximum and minimum shifted slightly to the right, and the recovery maximum appeared in the left mammary region, giving rise to patterns with three extrema (Fig. 32.17d). Later, only two extrema remained: the recovery minimum in the sternal or right mammary region and the recovery maximum in the left mammary area (Fig. 32.17e). This pattern persisted throughout the ST and T intervals (Fig. 32.17f) and approximately represented a mirror image of the potential distribution observed during the last phases of ventricular activation.

In some patients, a different behavior of the potential maximum and minimum was observed during the midportion of QRS; that is, the anterior maximum, after reaching the precordial area, did not complete its leftward migration but reverted to the sternal region and then moved to the right precordium, thereby taking over the role of the second maximum observed in typical RBBB. The second minimum did not appear in the left parasternal region to the right of the maximum, as in typical cases, but to its left, in the external part of the left mammary region. The electrophysiological mechanism giving rise to this peculiar sequence of potential patterns observed could not be identified.

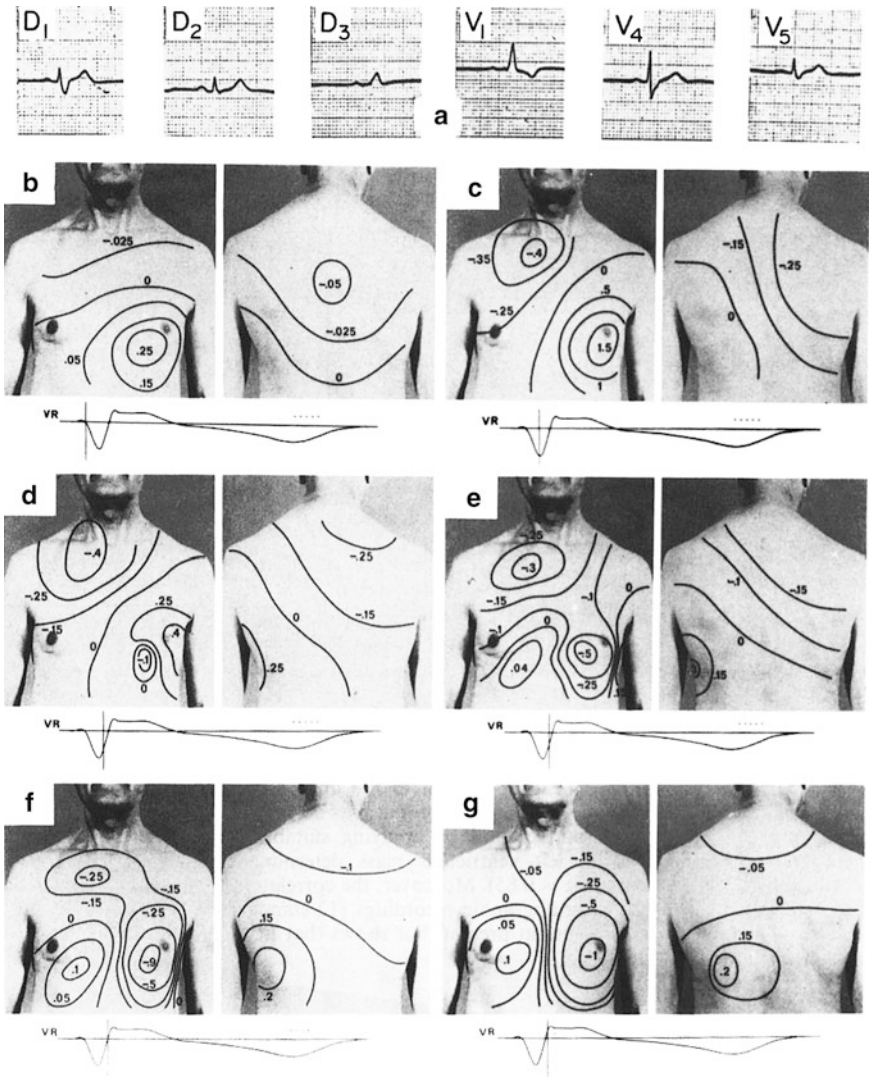

Figure 32.16

Subject with RBBB. (a) Standard ECG. (b–g) Each map refers to the instant of time indicated by the vertical line intersecting the reference ECG (VR). The values of equipotential lines are expressed in millivolts. (After Taccardi et al. [86]. © Churchill Livingstone, New York. Reproduced with permission.)

32.5.5 Left Bundle Branch Block

BSPMs have been described in uncomplicated left bundle branch block (LBBB), with or without left axis deviation [89–91] and in LBBB complicated by additional heart disease [90, 92].

In the uncomplicated LBBB studied by Musso et al. [90], at the onset of QRS (Fig. 32.18a), the potential maximum was consistently found in the sternal area. The minimum was generally located on the right chest, anteriorly or posteriorly. A few milliseconds later a new potential distribution developed, with a minimum in the presternal area and a maximum on the left mammary region. In some patients, the minimum migrated to the sternal area from its previous location. In other cases, an independent, secondary minimum appeared in this region and subsequently increased in magnitude, while the old minimum faded away. In both cases, the minimum settled in the sternal area earlier than in

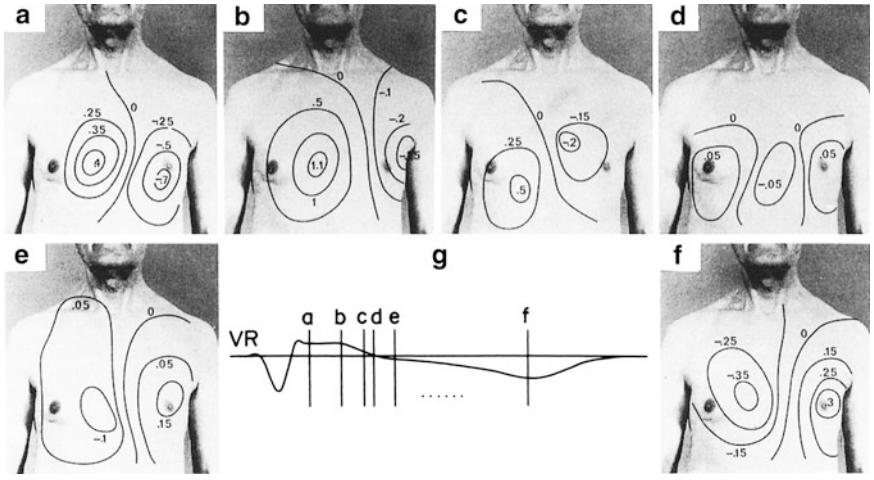

Figure 32.17

Same subject as in Fig. 32.16. BSPMs relating to second half of ventricular activation (a–d) and recovery (e, f). At instant d (end of QRS) recovery potentials are already present on the left side of the chest. (After Taccardi et al. [86]. © Churchill Livingstone, New York. Reproduced with permission.)

normal subjects. An early appearance of this minimum, which indicates right ventricular breakthrough, was also found by other investigators [91].

In LBBB, the initial phase of ventricular excitation differs from the normal sequence, in that the first electrical event occurring in the normal ventricles, that is, the excitation wavefront spreading through the septum from left to right and anteriorly, is missing. Therefore, ventricular excitation starts later than it would if the left bundle branch was functioning normally. As a consequence, the onset of ventricular activity as a whole is delayed in relation to His-bundle excitation.

The lack of left ventricular activity may explain the differences between the maps recorded in the early stages of QRS in LBBB patients and in normal subjects. The occurrence of the presternal minimum may be attributed, as in normal subjects, to the excitation wavefront reaching the right ventricular surface (right ventricular breakthrough). The shorter breakthrough time is not surprising since this time is calculated from the beginning of QRS, which is delayed in LBBB, as indicated above.

In the subsequent stages, the maximum moved to the left axilla, while the minimum persisted in the midsternal area. This distribution was a constant feature in the second half of QRS (Fig. 32.18b). In this interval, the potential maximum and minimum reached their peak value. However, the positive peak appeared later than the corresponding one in normal subjects. The surface patterns mentioned above can be related to the wide excitation wavefront, which, at these stages of the cardiac cycle, spreads through the septum from right to left and then invades the left ventricular walls.

In most cases of uncomplicated LBBB, 10–20 ms before the end of QRS a new maximum appeared in the upper sternal area (Fig. 32.18c). The maximum progressively increased in voltage and persisted throughout the ST-T interval. For this reason it was considered to be an early manifestation of the recovery process. The recovery minimum was located in the left axillary region (Fig. 32.18d), whence it generally moved toward the dorsal area at the end of the T wave. These events may be interpreted by inferring that (a) measurable repolarization potentials originate from the right ventricle before left ventricular depolarization is completed because the right ventricle is the first to depolarize and (b) the left ventricle behaves as a current sink during most of the recovery process, because of its delayed repolarization resulting from delayed activation.

Subjects with LBBB and left axis deviation described by Sohi et al. [91] differed from those with normal axes in that during the second half of the QRS interval, the maximum was generally located on the left shoulder and back. This pattern was attributed to a further selective slowing of depolarization in the anterobasal portions of the left ventricle.

BSPMs in complicated LBBB have been described by two groups of investigators [90, 92]. According to Preda et al. in LBBB associated with anterior MI, the middle third of the anterior chest wall remained negative during the final phases

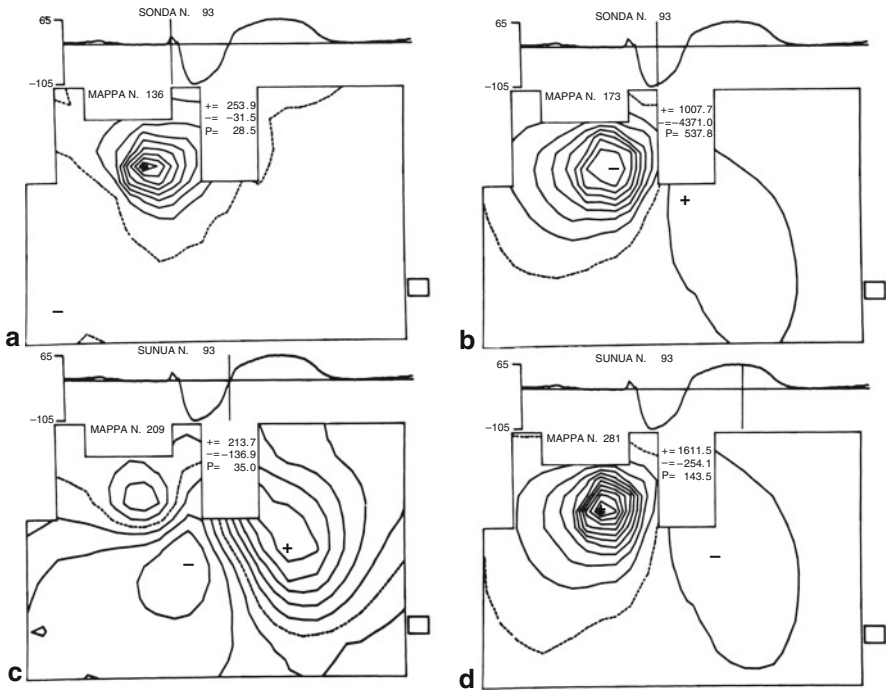

Figure 32.18

Patient with uncomplicated LBBB. BSPMs relating to four instants of time during ventricular excitation and recovery. The zero equipotential line is dashed. The plus and minus signs indicate the value of the positive and negative peaks (in microvolts). +P and −P indicate the step (in microvolts) between adjacent positive and negative equipotential lines.

of QRS. The authors attributed this finding to the lack of activation of the anterobasal region of the left ventricle, owing to the presence of the necrosis. In patients with infero-posterior MI, a persistent negativity was observed during the central portion of the QRS in the lower border of the chest, on the left lateral or posterior regions. Later, the negativity moved to the right side of the back. These findings were not confirmed by Musso et al. [90]. They studied LBBB complicated by anterior or inferior MI, LVH, myocardial ischemia, or a combination. By visually inspecting the maps, Musso et al. were unable to identify any potential pattern that could be uniquely found in a given LBBB group. However, several differences among groups were observed if the voltage values, rather than the potential patterns, were taken into account [90]. Generally, higher voltages were measured in patients with LVH and lower voltages were found in the MI groups as compared to uncomplicated cases of LBBB. These observations prompted Musso et al. to measure a set of voltage-related variables with a view to discriminating among different LBBB groups. The variables were derived by curves illustrating the behavior as a function of time during QRST of the highest instantaneous negative and positive potentials on the chest, the highest potential difference, the integral (extended to the entire chest surface) of the absolute value of the potential function, the size of the electropositive (or electronegative) thoracic areas, and so on. The statistical evaluation of the data (canonical variates analysis) permitted the classification of most complicated and uncomplicated patients into the correct group.

32.5.6 Left Anterior Fascicular Block

In left anterior fascicular block (LAFB), without MI or hypertrophy, one or more abnormal features could be detected in all patients. At the onset of QRS interval, in 8 out of 11 patients (unpublished data), the potential distribution was clearly abnormal in respect of (a) the location of the minimum, which was at a higher thoracic level with respect to the corresponding maximum, and/or (b) the anomalous position of the maximum (Fig. 32.19a). This potential pattern

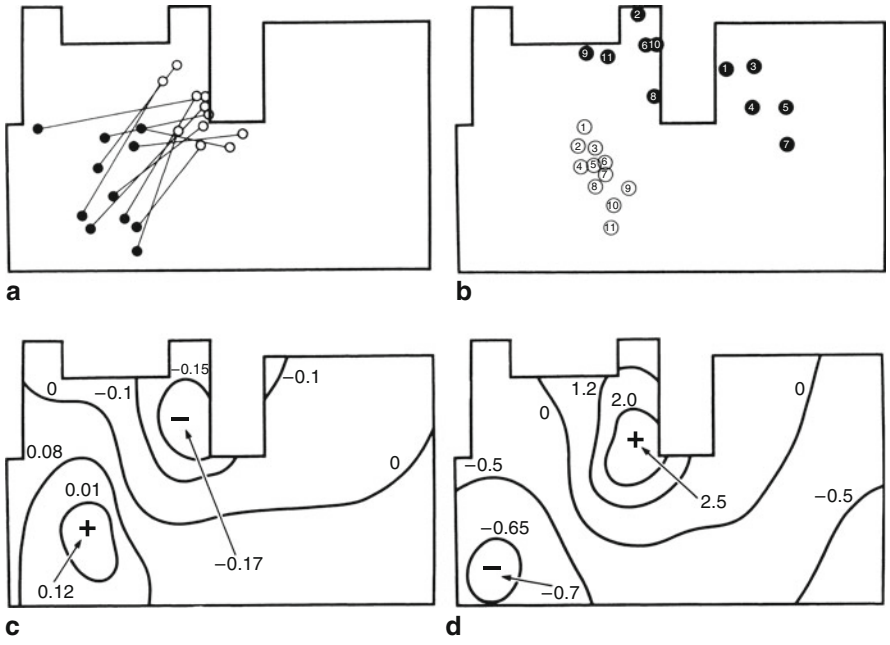

Figure 32.19

***Top*: Location of potential maxima (black circles) and minima (white circles) on the chest surface (a) at the onset of ventricular activation and (b) after 55 ms in 11 subjects with LAFB. The potential maximum and minimum relating to a given patient are indicated by the numbers inside the circles. *Bottom*: Subject with LAFB. Potential distribution at 10 ms (c) and at 46 ms (d) after the onset of ventricular activation. Potential values are expressed in millivolts.**

could be related to the direction of the activation wavefront, which spreads inferiorly and rightward. This anomalous direction is probably owing to the lack of early excitation of the anterosuperior portion of the left septal surface, as found in experimental studies [93].

During the mid- and late-QRS interval, a characteristic potential distribution was observed in all patients, by the authors and others [94]. After 28–30 ms from the onset of ventricular activation, the potential maximum was invariably located in the upper portion of the anterior or posterior chest surface, above the horizontal plane passing through the corresponding minimum (Fig. 32.19b). The minima clustered on the lower anterior chest wall (Fig. 32.19b) while the lower part of the chest was constantly electronegative. This potential distribution accounts for the left axis deviation in the standard ECG and can be attributed to the abnormal sequence of ventricular excitation in LAFB and particularly to the delayed activation of the anterosuperior part of the left ventricular wall.

The motion of the maximum to the upper thoracic areas occurred as follows. In 5 cases out of 11, the maximum did not migrate to the back, as in normal subjects, but moved directly from the left mammary region to the upper sternal or left clavicular areas. In the remaining six cases, it moved to the back and remained there (five cases) or reached the anterior left shoulder. It is suggested that in those patients where the maximum moved dorsally, a lesser degree of asynchronism existed between the activation of the posterior and anterior basal portions of the left ventricle. The variety of patterns observed may result from different degrees of delay in the anterior fascicle and/or from individual variations in the anatomical distribution of the peripheral conducting fibers.

32.5.7 Wolff–Parkinson–White Syndrome

It is well known that the Wolff–Parkinson–White (WPW) syndrome is a result of the early excitation of some portions of the ventricles through anomalous conduction pathways. These can be found at almost any location around the AV

ring, including the ventricular septum. Conventional ECGs and VCGs provide useful information on the orientation and direction of propagation of the pre-excitation wavefront, but they do not enable the location of the pre-excited area to be determined reliably. A number of investigations have shown that much more information on the location of the pre-excitation focus can be gained by measuring the instantaneous potential distribution on the entire chest surface [95–102].

Yamada et al. described three types of surface maps in 22 WPW patients on the basis of QRS potential distributions [95]. Type I potential patterns were ascribed to pre-excitation of the posterior aspect of the left ventricle, type II to pre-excitation of the basal part of the right ventricle, and type III to pre-excitation in the proximity of the posterior right AV groove close to the ventricular septum.

In a group of 42 WPW patients, De Ambroggi et al. [96] were able to recognize six types of maps, on the basis of the following considerations and criteria, derived mainly from previous studies on physical, mathematical, and physiological models [1, 103, 104].

At the onset of the delta wave, the pre-excitation wavefront is small and can be approximated by a single equivalent dipole, at least as far as surface potential patterns are concerned. When the two potential extrema on the body surface have nearly equal strength, the dipole is equidistant from the surface extrema and its depth in the chest is proportional to the distance between the extrema. When one extremum is stronger than the other, the dipole is closer to the stronger extremum. The direction of the dipole is approximated by a straight line joining the two extrema. After the delta wave, the body-surface potential patterns are not clearly related to the location of the pre-excitation wavefront. However, the appearance of a sternal minimum indicating a normal right ventricular breakthrough may suggest a left or posterior localization. On the basis of these simple rules, we proposed the following classification of the patients studied.

Type 1 (Figs. 32.20a, 32.21). During the delta wave, the maps of the 23 patients belonging to type 1 exhibited a potential maximum on the precordial area and a minimum on the back. It is suggested that the pre-excitation wave was located deep in the thorax, most likely in the posterobasal wall of the heart and spread in a postero-anterior direction. Between 40 and 90 ms after the onset of ventricular activation, a second minimum appeared on the sternal area in most patients, while the dorsal minimum reached the upper anterior chest wall. The second minimum was attributed to the right ventricular breakthrough. Its appearance suggested that the right anterior ventricular wall was excited through the normal pathways and was therefore not affected by pre-excitation.

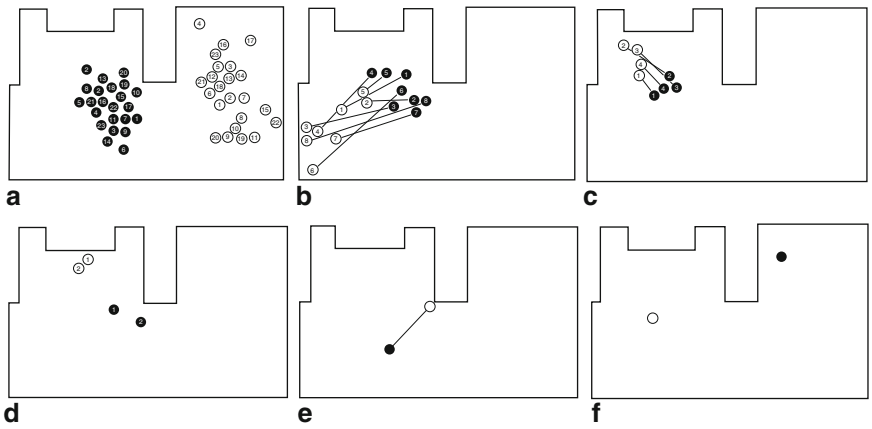

Figure 32.20

Location of potential maxima (black circles) and minima (white circles) on the chest surface during the delta wave in WPW patients belonging to type 1(a), 2(b), 3(c), 4(d), 5(e), and 6(f). The potential maximum and minimum relating to a given patient are indicated by the numbers inside the circles. (After De Ambroggi et al. [96]. © American Heart Association, Dallas, Texas. Reproduced with permission.)

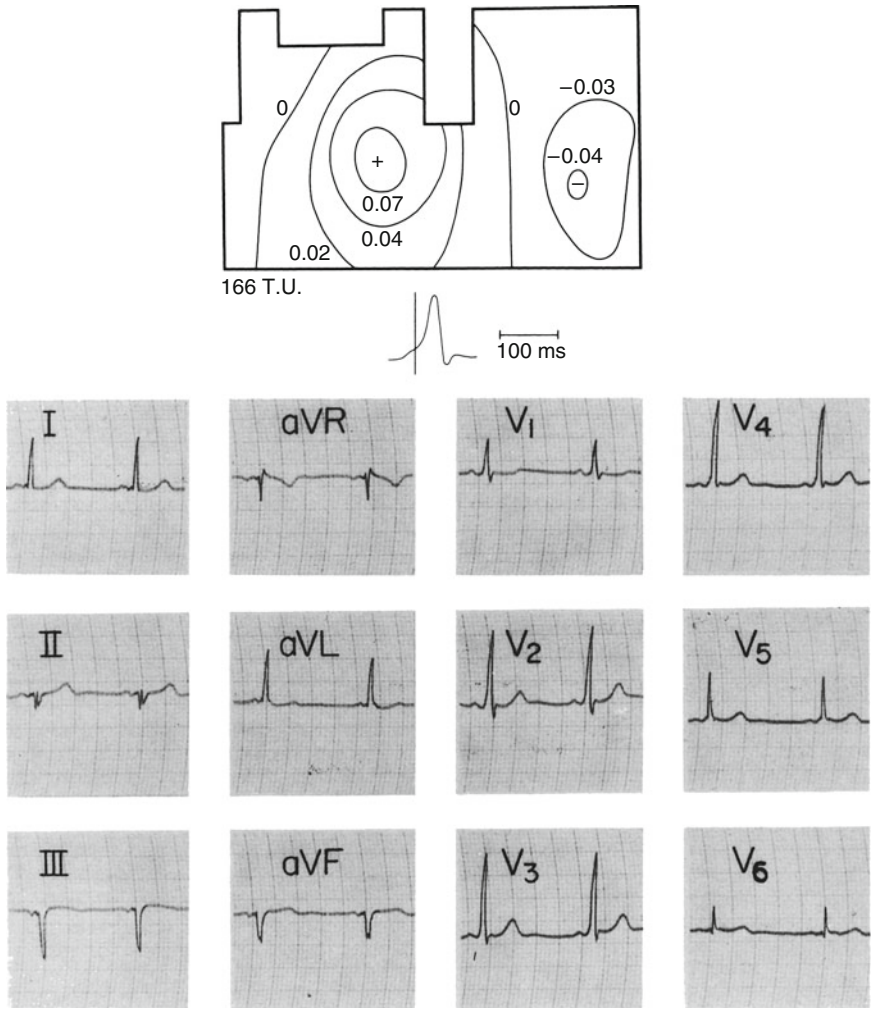

Figure 32.21

BSPM during the delta wave, at the instant indicated by the vertical line crossing the reference ECG in a WPW subject belonging to type 1. The 12-lead ECG shows a type A WPW pattern. (After De Ambroggi et al. [96]. © American Heart Association, Dallas, Texas. Reproduced with permission.)

Type 2 (Figs. 32.20b, 32.22). During the delta wave, in the eight patients belonging to type 2, the minimum was located on the inferior half of the right anterior chest wall and the maximum on the sternal or left mammary region. The location of the minimum and maximum suggests that the pre-excitation wave moved leftward and upward and probably spread from the lateral inferior portion of the AV groove through the right ventricular wall. In no patient of this group did a second minimum appear on the sternal area. This suggested that the right ventricular wall was not activated through the normal conducting pathways.

Type 3 (Figs. 32.20c, 32.23). During the delta wave in the four type-3 patients, the minimum was initially on the back and then moved to the right subclavicular area; the maximum was located in the mid-sternal area. This potential distribution suggested that an excitation wave was spreading through the anterior wall of the right ventricle from the upper part of the right AV groove, downwards and to the left. A second minimum did not appear in the sternal area in the patients of this group, suggesting that the right ventricular wall was not excited through the normal pathways.

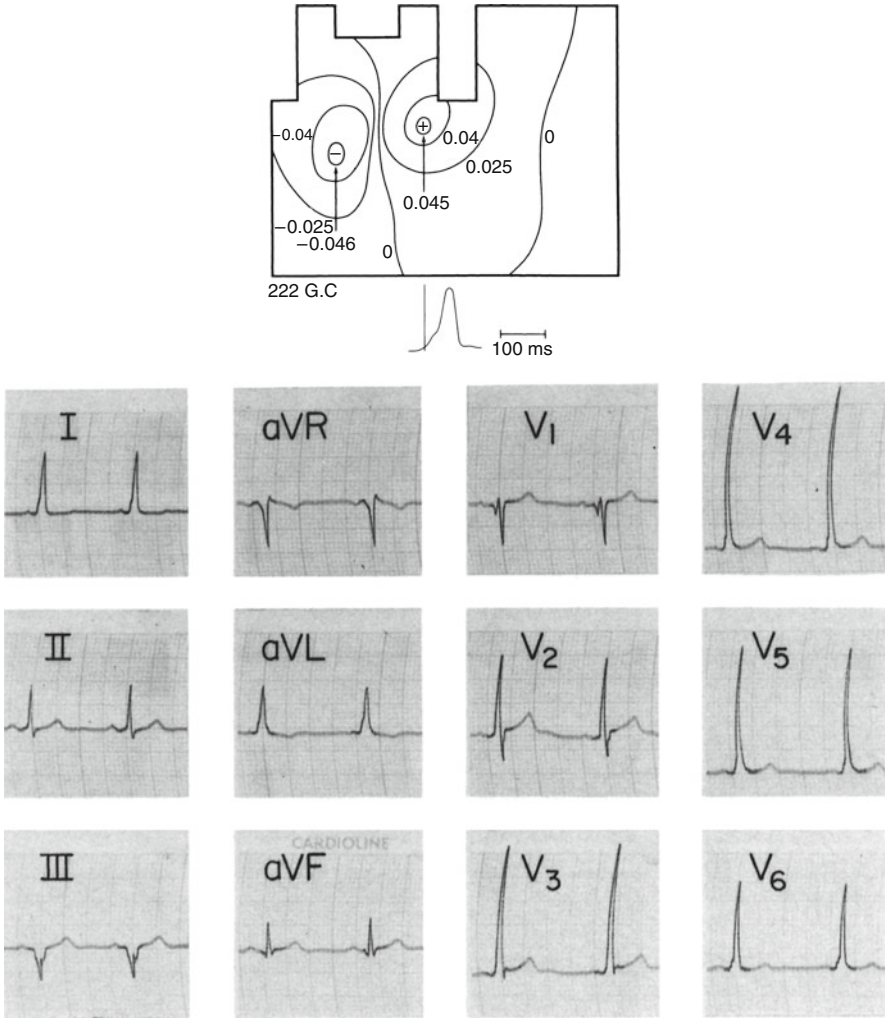

Figure 32.22

BSPM during the delta wave in a WPW patient belonging to type 2. The ECG shows a type B WPW pattern. (After De Ambroggi et al. [96]. © American Heart Association, Dallas, Texas. Reproduced with permission.)

Type 4 (Fig. 32.20d). Two patients were classified as type 4. During the delta wave, both the maximum and minimum were located on the left anterior chest wall, with the maximum being on the mammary region, and the minimum on the upper sternal area. This potential distribution suggested that pre-excitation probably started in the anterior portion of the left AV groove or in the anterior portion of the septal AV ring, spreading toward the apex of the left ventricle. A right-sided location was unlikely since neither extreme was on the right-chest surface. In agreement with this interpretation, a second minimum appeared on the sternal area in one patient. This minimum indicated a normal right ventricular breakthrough and showed that pre-excitation did not involve the anterior wall of the right ventricle. In the other patient, there was no second minimum; this patient, however, exhibited a sequence of surface potentials indicating right bundle branch block, which usually prevents the appearance of the sternal minimum.

Type 5 (Fig. 32.20e). Type 5 was represented by a single subject. The potential minimum was located in the left axillary region and the maximum on the inferior part of the left anterior chest wall. This potential distribution indicated

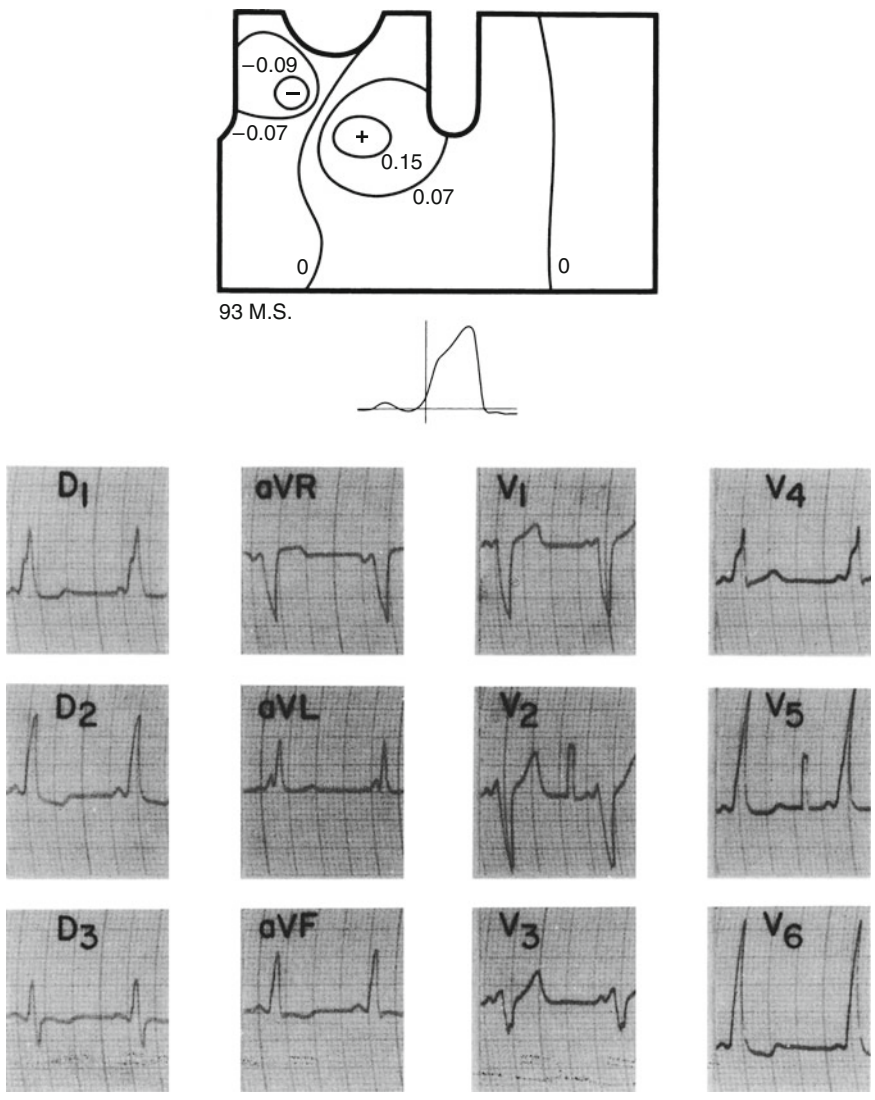

Figure 32.23

BSPM during the delta wave in a patient belonging to type 3. The ECG shows a type B WPW pattern. (After De Ambroggi et al. [96]. © American Heart Association, Dallas, Texas. Reproduced with permission.)

that pre-excitation most probably spreads through the left ventricular wall, starting from the anterolateral portion of the left AV groove and then moving downward and to the right.

Type 6 (Fig. 32.20f). Type 6 was also represented by a single patient. The ECG showed an unusual pattern of ventricular pre-excitation. A delta wave was not clearly detectable; a small Q wave was present in V1 and the QRS duration was within normal limits. Intracardiac recordings showed a short HV interval but during ajmaline administration, the Q wave in V1 disappeared and the HV interval rose from 15 to 40 ms. At the onset of ventricular excitation, the potential distribution was characterized by a minimum at the right lower sternal border and a maximum on the left scapular area. Twenty five minutes after the onset of ventricular activation, a normal sequence of potential patterns was observed. The initial location of the minimum and maximum indicated that an excitation wave was probably spreading in an antero-posterior direction, leftward and slightly superiorly. An acceptable location for such a wavefront might be in the right

side of the interventricular septum. The most likely mechanism for right septal pre-excitation would be through Mahaim fibers, stemming from the initial part of the right bundle branch.

In a number of patients belonging to types 1, 2, 3, 5, and 6, the site of pre-excitation as deduced from surface maps was in good agreement with that independently established using intracardiac recordings, epicardial maps, or surgical results [105].

Benson et al. [99] attempted to localize the site of pre-excitation in 49 WPW patients, where the location of the anomalous pathway was determined by intracardiac electrophysiological studies or surgical ablation. These authors were able to predict accurately at least seven pre-excitation sites on the basis of surface potential distribution during the QRS (at 40 ms after the onset of delta wave) and ST segment. Moreover, they found the potential distribution during early ST segment more useful than QRS maps for localizing the pre-excited area. Their classification was in reasonably good agreement with our classification previously presented.

Kamakura et al. [100] studied 41 WPW patients to determine the most reliable index for predicting the site of a single accessory pathway. They found that the location of the ventricular insertion of the accessory AV connection (determined at electrophysiological study or during surgery) is well estimated at the time the amplitude of the negative surface potential is −0.15 mV. On the basis of the chest position of the minimum with a potential of −0.15 mV, the location of the accessory AV connection was correctly predicted in 36 of 41 cases.

Liebman et al. [101] recorded BSPM in 34 patients with WPW syndrome in whom the site of ventricular insertion of the anomalous AV connection was localized by an electrophysiologic study and, in 18 cases, at surgery. Attempts were made to identify the 17 ventricular insertion sites along the AV grove described by Guiraudon et al. [106] mainly using QRS analysis (location of the initial minimum, occurrence of right ventricular breakthrough). The ventricular insertion sites determined by BSPM and EPS at surgery were identical or within one mapping site (i.e., 1.5 cm or less) in 14 of 18 cases; three of the four exceptions had more than one accessory AV connection, and the other had a very broad ventricular insertion. BSPM and EPS locations of accessory pathways correlated very well in the 34 cases despite the fact that BSPM determined the ventricular insertion and EPS the atrial insertion site of the accessory AV connection. BSPMs of QRS were very accurate in predicting the right ventricular versus left ventricular postero-septal AV connections, known to be particularly difficult at EPS in three of four surgical cases. Typical right ventricular breakthrough occurs in all patients with left ventricular free wall accessory connections, but was not observed in cases with right ventricular free wall or anteroseptal accessory AV connections.

In 1993, Dubuc et al. [102] reported on the use of BSPM to guide catheter ablation of accessory AV connection in 30 WPW patients. The catheter used for radiofrequency ablation was first placed in the vicinity of the ventricular pre-excitation site predicted by BSPMs previously recorded during the delta wave. BSPMs were then recorded during pacing with this catheter; the comparison between the pre-excited and paced BSPMs indicated whether the pacing site was too anterior or posterior with respect to the pre-excitation site, and the catheter was moved accordingly. This process was repeated until the pre-excited and paced BSPMs were almost identical, i.e., showed high correlation coefficient (>0.8) during the delta wave, and ablation was then attempted. In this way, it was possible to successfully ablate the accessory pathway in 93% of cases.

32.5.8 Arrhythmogenic Cardiopathies

32.5.8.1 Postinfarction Ventricular Tachycardias: Identification of Site of Origin of Ventricular Tachycardias

Extensive investigations were made by Sippens-Groenewegen et al. to assess the value of BSPMs in localizing the site of origin of ectopic ventricular activation in patients with a structurally normal heart and with myocardial infarction [107–109]. In patients with normal cardiac anatomy, the QRS maps allowed discrimination among 38 different LV and RV segments of ectopic endocardial impulse formation [107]. The use of 62 lead BSPMs instead of the 12-lead ECG during endocardial pace mapping technique enhanced the localization resolution of this technique and thus enabled more precise identification of the site of origin of postinfarction VT episodes [108].

In patients with previous anterior and inferior myocardial infarction, the same authors demonstrated that QRS integral maps enabled a precise localization of the origin of postinfarction ventricular tachycardia in 62% and regional

approximation (identification of a segment immediately adjacent to the actual endocardial segment of origin) in 30% of tachycardias [109].

More recently, McClelland et al [110] were able to compute epicardial potentials from BSPM (80 leads) using an inverse solution method. They were able to reconstruct in 5 patients epicardial isochronal maps demonstrating the exit site and the re-entry circuit of ventricular tachycardias.

32.5.8.2 Susceptibility to Ventricular Arrhythmias

Eigenvector analysis [111] was applied to QRST integral maps of two groups of patients with old myocardial infarction (11 patients with episodes of sustained ventricular tachycardia and 62 without arrhythmias) and in a control group of healthy subjects [112]. This method makes possible the detection and quantification of nondipolar components not evident on visual inspection of the integral maps. The cumulative contribution of the eigenvectors beyond the third to an individual map, expressed as percentage contribution of the total map content, has been considered a "nondipolar content" of that map. On average, the nondipolar content was significantly greater in patients with MI than in controls (8.3 ± 6.4% vs 4.1 ± 2.2%, $p < 0.001$) and, among patients, in those with ventricular tachycardia (7.2 ± 5.3% vs 16.6 ± 8.5%, $p < 0.001$). These findings were in agreement with those reported by Abildskov et al. [113]. Thus, the high nondipolar content of QRST maps in patients with ventricular tachycardia suggests the presence of local disparities of repolarization and it may be considered a useful marker of susceptibility to malignant arrhythmias.

Hubley-Kozey et al. [114] derived 16 eigenvectors from the total set of 204 QRST maps (102 patients with ventricular tachyarrhythmias and 102 patients without) but did not find a statistically significant difference in dipolar content between the two groups (13.1 ± 9.7 vs 12.9 ± 10.2%, $p > 0.05$). Because the nondipolar content did not perform well in their study population, the authors examined how individual eigenvector patterns contribute to QRST integral maps in each group of patients. Statistically significant differences were found between the values of Karhunen-Loeve coefficients in VT and non-VT groups for the 6th, 4th, 13th, 5th, 1st, 2nd, and 11th eigenvectors, in order of significance levels. Using stepwise discriminant analysis, they selected features subsets that best discriminated between the two groups. For an optimal set of eight spatial features, the sensitivity and specificity of the classifier for detecting patients with VT in 1,000 test sets were 90 ± 4% and 78 ± 6%, respectively. The authors concluded that the multiple body-surface ECGs contain valuable spatial features that can identify the presence of an arrhythmogenic substrate in the myocardium of patients at risk of ventricular arrhythmias.

Recently, Korhonen et al. [115] studied the complexity of T-wave morphology in BSPM of patients with recent myocardial infraction and cardiac dysfunction, by applying principal component analysis. They found that the 3rd principal component derived from BSPM was a significant predictor of arrhythmic events in this population.

32.5.8.3 BSPM and Ventricular Late Potentials

Vulnerability to arrhythmias has also been related to the existence of areas of delayed conduction at the end of the ventricular activation process. Ventricular late potentials recorded on signal-averaged ECG are the expression of this phenomenon. BSPM can be applied to detect these high-frequency, low-amplitude potentials [116, 117]. Maps not only made it possible to reveal the presence of late potentials, but also to determine the spatial distribution of late potentials in patients with ventricular tachycardia. Thus, BSPM may provide additional information about the thoracic location of ventricular late potentials, which can be related to the sites of conduction delay and possibly to the sites of origin of ventricular tachycardia.

32.5.8.4 Long QT Syndrome

BSPMs in patients with idiopathic long QT syndrome were described by De Ambroggi et al. [118]. No peculiar features were observed during the QRS interval, while the ventricular repolarization presented some abnormalities in addition to QT prolongation.

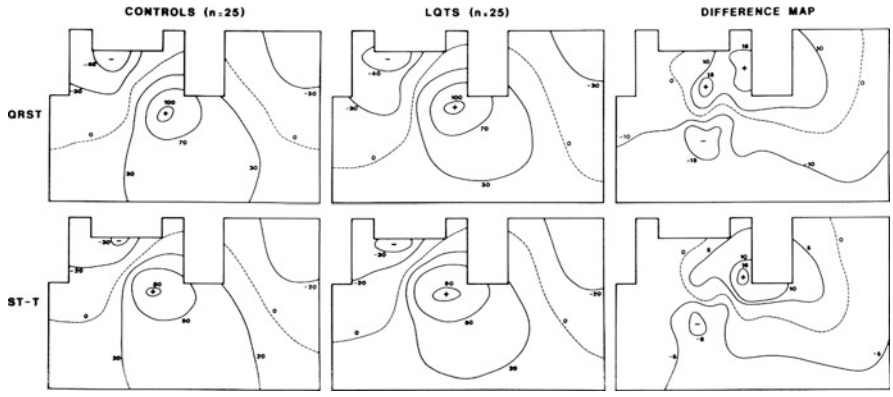

Figure 32.24

Mean integral maps of QRST and ST-T intervals in the control and LQTS groups. Difference maps are illustrated in the third column. Values are expressed in μVs. (After De Ambroggi et al. [118]. © American Heart Association, Dallas, Texas. Reproduced with permission.)

The visual inspection of instantaneous BSPMs revealed that the potential distributions were grossly abnormal (location of the potential extrema, presence of multiple peaks) in only a few cases. On the other hand, in most patients, BSPMs revealed less marked abnormalities in the instantaneous potential distribution. For instance, in several patients the negative potentials during the entire repolarization covered an area on the anterior thorax larger than in control subjects.

Differences between normals and LQTS patients were better quantified by analyzing ST-T and QRST integral maps. The mean integral map from the LQTS patients showed a potential distribution similar to that of the mean integral map from the control subjects. Nevertheless, the difference map (LQTS mean map minus control mean map) showed that LQTS patients had lower values on the inferior half of the trunk and on the right anterior thorax and higher values on the left anterior thorax compared with control subjects (Fig. 32.24). In 13 patients, the negative values covered almost entirely the right anterior thorax. In six patients, there was a multipeak distribution of the integral values. The prominent negative area on the anterior chest in LQTS patients could result from a delayed repolarization of the underlying anterior wall so that it remains electronegative longer than other cardiac regions. Moreover, the multipolar distribution may reflect local inequalities in recovery times. ST-T integral maps were substantially similar to QRST maps, but a multipolar distribution was observed in a few more patients.

Eigenvector analysis [111] was also applied to QRST and ST-T integral maps. As already mentioned, this method makes possible the detection and quantification of nondipolar components not evident on visual inspection of the integral maps. The percent contribution of nondipolar eigenvectors (all eigenvectors beyond the third) to maps was significantly higher in LQTS patients than in normals. Moreover, eight patients who had a high nondipolar content did not show a multipeak distribution on their integral maps. This demonstrates that eigenvector analysis can detect nondipolar components not evident on integral maps.

To identify markers of dispersion of the ventricular repolarization, in a subsequent investigation on 40 patients with LQTS [119], we applied principal component analysis to all the recorded ST-T waves in each subject studied. We defined the ratio between the information content of the first principal component and the total information of the original data as "similarity index." Actually, a high value of similarity index indicates a great similarity of all waveforms to one fundamental waveform, that is, a great similarity of all waves to each other. On the contrary, a low value of similarity index indicates a large variety of ST-T waves and is considered a marker of repolarization disparities. In the 40 patients affected by congenital LQTS [119], the mean value of the similarity index was significantly lower than in healthy control subjects (49 ± 10 vs $77 \pm 8\%$, $p < 0.0001$). A value lower than 61%, corresponding to two standard deviations below the mean value for controls, was found in 35 of 40 patients and in only one control subject (sensitivity 87%, specificity 96%). In our experience, the similarity index has proved to be a more sensitive marker than multipolar distribution of QRST integral maps in revealing electrical disparities of ventricular repolarization.

32.5.8.5 Arrhythmogenic Right Ventricular Cardiomyopathy

Characteristic features of BSPMs were described in patients with arrhythmogenic right ventricular cardiomyopathy (ARVC). De Ambroggi et al. studied 22 patients affected by ARVC, nine with episodes of sustained ventricular tachycardias (VT) and 13 without [120]. The QRST integral maps showed in most ARVC patients a larger than normal area of negative values on the right anterior thorax. This abnormal pattern could be explained by a delayed repolarization of the right ventricle. Nevertheless, it was not related to the occurrence of VT in our patient population. To detect minor heterogeneities of ventricular repolarization, the principal component analysis was applied to the 62 ST-T waves recorded in each subject. We assumed that a low value of the first or of the first three components (Co 1, 2, 3) indicates a greater than normal variety of the ST-T waves, a likely expression of a more complex recovery process. The mean values of the first three components were not significantly different in ARVC patients and in control subjects. Nevertheless, considering the two subsets of patients with and without VT, the values of Co 1, of Co 1 + 2, and of Co 1 + 2 + 3 were significantly lower in the group of ARVC patients with VT. Values of Co 1 < 69% (equal to one SD below the mean value for controls) were found in six of nine VT patients and in one patient without VT (sensitivity 67%, specificity 92%). A low value of Co 1 was the only variable significantly associated with the occurrence of VT.

QRST integral maps with an abnormal negative area on the anterior thorax were also observed by Peeters et al. [121] in eight out of eight patients with ARVC, but in only two of eight patients with idiopathic right ventricular tachycardia.

32.5.8.6 Brugada Syndrome

The Brugada syndrome is a familial, "primary" electrical disease of the heart due to gene mutations encoding for the sodium channel and is characterized by a delayed activation of the right ventricle, with a QRS complex resembling that of right bundle branch block in V1, early ST elevation (J wave) in the right precordial leads, normal QT duration, inducibility of ventricular tachycardia, and a high risk of sudden cardiac death [122].

ECG changes have been quantified by 120-lead BSPMs: the QRS integrals were higher over the upper-right precordium and lower than normal over the lower left precordium; steeper negative ST gradients compared to normal were present over the upper left precordium and more positive ST gradients compared to normal over the lower left precordium [123].

Early ST elevation ($\geqslant$0.2 mV) was observed on a variable area over the right precordium. If this area is larger than 50 cm^2, it has a 92% positive and a 62% negative predictive value for inducibility of ventricular tachycardia, but similar predictive power was found for ventricular late potentials in the same patients [124].

Amplitude of maximal ST elevation was also used to differentiate Brugada syndrome patients with inducible ventricular tachycardia from asymptomatic patients [125].

32.6 Conclusions

The most general advantage of BSPMs is the fact that they record cardiac potentials from broad areas of the chest, thus enabling the detection of significant physiologic and possibly diagnostic information outside the precordial regions usually explored. Moreover, BSPMs provide the spatial as well as the temporal and amplitude components of cardiac electrical activity, whereas the ECG scalar waveforms present only the voltage variation with time in a given site.

As reported in the previous pages, investigations by different authors so far published clearly demonstrated a higher diagnostic content of BSPMs, compared with conventional ECG, in various pathological conditions.

Nevertheless, a widespread or even limited clinical application beyond the research laboratories of BSPM has not occurred up to day for several reasons: (a) the recording and processing of large numbers of leads and the displaying of maps have been complex and time-consuming, (b) a completely automated instrumentation was not commercially available, (c) use of many lead systems in different laboratories, differing in the number and placement of leads, and (d) difficulty in interpreting BSPM. The last reason is probably the most important obstacle that hampers the clinical use of BSPM.

In recent years, some of these obstacles have been overcome. BSPM recording systems, even those not widely marketed, have been (and can) relatively easily be developed and produced by several laboratories. Today's computer facilities make the recording and the data analysis easier than in the past. The time for applying electrodes and for data acquisition and analysis has been reduced considerably. Procedures, which reduce the number of leads that are necessary for reconstructing surface maps without losing too much information, have also been proposed; among these, the 32-lead system of Lux is the most commonly used [126]. Moreover, methods for converting multilead ECGs from one lead system to another have been proposed and satisfactorily applied [10].

The problem of interpreting surface maps still remains; in general, it may be approached essentially in two ways. The first approach is based on statistical methods, that is, defining the normal variability range of a number of parameters derived from maps relating to healthy subjects of different age, sex, and body shape, and then comparing these parameters by means of multivariate statistical procedures with those recorded from patients. The second approach is "deterministic"; that is, it consists of establishing the relationships between the intracardiac current sources (i.e., number, shape, location, and motion of excitation wavefronts and sequence of repolarization) and surface potential distribution (i.e., number, location, and motion of potential maxima and minima). This can be made in different ways, by using physiological or mathematical models. For instance, the distribution of currents and potentials has been determined experimentally in conducting media surrounding isolated hearts [127] thus enabling epicardial potentials to be compared with potentials recorded at a distance from the heart. Intracardiac current sources of known location have been produced by simultaneously stimulating the heart at multiple sites [128]. This allowed surface potential patterns to be correlated with known distributions of generators. The relationships between epicardial and body-surface potentials during activation and recovery were studied in intact chimpanzees [129, 130] and mathematical procedures for solving the direct and inverse problem (i.e., calculating surface potentials from internal sources and vice versa) were proposed by different authors (see Chaps. 8 and 9).

In the intact dog, Spach et al. succeeded in calculating accurately body-surface potentials from epicardial potential distributions during activation and recovery [131]. As regards the inverse problem, epicardial potentials have been calculated from potential distributions at the body surface in dogs [132–137]. In this respect, particularly important are the studies of Rudy and coworkers. They demonstrated the ability to compute noninvasively epicardial potential distribution and epicardial activation sequences from measured surface potentials. They called this new electrocardiographic modality as "ECG imaging," which, of necessity, has to utilize BSPM recording. The ECG imaging has been successfully applied in humans [138–141], using geometrical information from computed tomography and a mathematical algorithm, in different situations including the normal heart, a heart with a conduction disorder (right bundle branch block), focal activation initiated by right or left ventricular pacing, focal atrial tachycardia and flutter. A simplified method of inverse solution, which adopts a general torso model in which the same anatomic data are used irrespective of the body habitus, was applied by McClelland et al [110]. Despite these limitations they were able to reconstruct epicardial potential or isochronal maps identifying the left ventricular pacing site or indicating the exit site and the re-entry circuit of ventricular tachycardias. Very recently improvements to the inverse solution method were made by A. van Oosterom and coworkers [142]. The required computation time and the quality of the results obtained should favour the applications of this inverse procedure in a clinical setting.

In addition to all the reasons discussed above, the lack of expansion in the clinical setting of BSPM, which indeed can be considered an "advanced electrocardiographic method," is partially due to the fact that electrocardiology in recent years has lost some of its importance compared with newer sophisticated imaging techniques. The anatomic and functional information on several heart conditions (e.g., hypertrophy, location and extension of myocardial infarction, and so on) that, in the past, was obtained with varying degrees of accuracy by means of electrocardiographic techniques, can be more precisely and directly obtained today by other techniques such as echocardiography, magnetic resonance, multislice computed tomography, and nuclear imaging. On the other hand, electrocardiology still has a unique, primary role in the field of arrhythmias and conduction disturbances, into which no other technique can provide relevant insights. In particular, ECG imaging, based on the solution of the "inverse problem," which is the final aim of electrocardiography, hopefully will be able in the near future to provide, noninvasively, information on the epicardial and intramural excitation and recovery processes. This could give the possibility of identifying, with sufficient accuracy, intramural heterogeneities, transmural re-entry and intramural focal arrhythmias, and of defining ischemic or necrotic areas within the myocardium. The future of body-surface potential maps should be in that direction.

References

1. Plonsey, R., *Bioelectric Phenomena*. New York: McGraw-Hill, 1969, pp. 202.
2. Colli Franzone, P., L. Guerri, C. Viganotti, et al., Potential fields generated by oblique dipole layers modeling excitation wavefronts in the anisotropic myocardium. Comparison with potential fields elicited by paced dog hearts in a volume conductor. *Circ. Res*., 1982;**51**: 330–346.
3. Taccardi, B., E. Macchi, R.L. Lux, et al., Effect of myocardial fiber direction on epicardial potentials. *Circulation*, 1994;**90**: 3076–3090.
4. Yan, G.X. and C. Antzelevitch, Cellular basis for the normal T wave and the electrocardiographic manifestations of the long QT syndrome. *Circulation*, 1998;**98**: 1928–1936.
5. Antzelevitch, C., W. Shimitzu, G.X. Yan, et al., The M cells: its contribution to the ECG and to normal and abnormal electrical function of the heart. *J. Electrophysiol*., 1999;**10**: 1124–1152.
6. Waller, A.D., On the electromotive changes connected with the beat of the mammalian heart and of the human heart in particular. *Philos. Trans. R. Soc. Lond. Ser. B*, 1889;**180**: 169–194.
7. Nahum, L.H., A. Mauro, H.M. Chernoff, and R.S. Sikand, Instantaneous equipotential distribution on surface of the human body for various instants in the cardiac cycle. *J. Appl. Physiol*., 1951;**3**: 454–464.
8. Taccardi, B., Distribution of heart potentials on dog's thoracic surface. *Circ. Res*., 1962;**11**: 862–869.
9. Taccardi, B., Distribution of heart potentials on the thoracic surface of normal human subjects. *Circ. Res*., 1963;**12**: 341–352.
10. Hoekema, R., G.J.H Uijen, D. Stilli, and A. van Oosterom, Lead system transformation of body surface map data. *J. Electrocardiol*., 1998;**31**: 71–82.
11. Abildskov, J.A., M.J. Burgess, P.M. Urie, R.L. Lux, and R.F. Wyatt, The unidentified information content of the electrocardiogram. *Circ. Res*., 1977;**40**: 3–7.
12. Abildskov, J.A., M.J. Burgess, R.L. Lux, R.F. Wyatt, and G.M. Vincent, The expression of normal ventricular repolarization in the body surface distribution of T potentials. *Circulation*, 1976;**54**: 901–906.
13. Corlan, A.D., R.S. Macleod, and L. De Ambroggi, The effect of intrathoracic heart position on ECG autocorrelation maps. *J. Electrocardiol*., 2005;**38**: 87–94.
14. Taccardi, B., Body surface distribution of equipotential lines during atrial depolarization and ventricular repolarization. *Circ. Res*., 1966;**19**: 865–878.
15. Taccardi, B., L. De Ambroggi, and C. Viganotti, Body-surface mapping of heart potentials, in *The Theoretical Basis of Eleclrocardioiogy*, C.V. Nelson and D.B. Geselowitz, Editors. Oxford: Clarendon, 1976, pp. 436–466.
16. Mirvis, D.M., Body surface distribution of electrical potential during atrial depolarization and repolarization. *Circulation*, 1980;**62**: 167–173.
17. Spach, M.S., R.C. Ban, R. Warrcn, D.W. Benson, A. Walston, and S.H. Edwards, Isopotential body surface mapping in subjects of all ages: emphasis on low-level potentials with analysis of the method. *Circulation*, 1979: **59**: 805–821.
18. Spach, M.S., T.D. King, R.C., O.E. Barr Boaz, M.N. Morrow, and S. Hennan-Giddens, Electrical potential distribution surrounding the atria during depolarization and repolarization in the dog. *Circ. Res*., 1969;**24**: 857–873.
19. Eddlemon, C.O., V.J. Rucsta, L.G. Horan, and D.A. Brody, Distribution of heart potentials on the body surface in five normal young men. *Am. J. Cardiol*., 1968;**21**: 860–870.
20. Young, B.D., P.W. Macfarlane, and T.D.V. Lawrie, Normal thoracic surface potentials. *Cardiovasc. Res*., 1974;**8**: 187–193.
21. Green, L.S., R.L. Lux, C.W. Haws, R.R. Williams, S.C. Hunt, and M.J. Burgess, Effects of age, sex, and body habitus on QRS and ST- T potential maps of 1100 normal subjects. *Circulation*, 1985;**71**: 244–253.
22. Spach, M.S., W.P. Silberberg, J.P. Boineau, et al., Body surface isopotential maps in normal children, ages 4 to 14 years. *Am. Heart. J*., 1966;**72**: 640–652.
23. Liebman, J., C.W. Thomas, Y. Rudy, and R. Plonsey, Electrocardiographic body surface potential maps of the QRS of normal children. *J. Electrocardiol*., 1981: **14**: 249–260.
24. Tazawa, H and C. Yoshimoto, Electrocardiographic potential distribution in newborn infants from 12 hours to 8 days after birth. *Am. Heart. J*., 1969;**78**: 292–305.
25. Benson, D.W. Jr. and M.S. Spach, Evolution of QRS and ST-T-wave body surface potential distributions during the first year of life. *Circulation*, 1982;**65**: 1247–1258.
26. Durrer, D., R.Th van Dam, G.E. Freud, M.J. Janse, F.L. Meijler, and R.C. Arzbaecher, Total excitation of the isolated human heart. *Circulation*, 1970;**41**: 899–912.
27. Wyndham, C.R., M.K. Meeran, T. Smith, et al., Epicardial activation of the intact human heart without conduction defect. *Circulation*, 1979;**59**: 161–168.
28. Green, L.S., R.L. Lux, D. Stilli, C.W. Haws, and B. Taccardi, Fine details in body surface potential maps: accuracy of maps using a limited lead array and spatial and temporal data representation. *J. Eleclrocardiol*., 1987;**20**: 21–26.
29. Hoekema, R., G.J. Uijen, and A. Van Oosterom, Geometrical aspects of the interindividual variability of multilead ECG recordings. *IEEE Trans. Biomed. Eng*., 2001;**48**: 551–559.
30. Kozmann G, R.L. Lux, and L.S. Green, Sources of variability in normal body surface potential maps. *Circulation*, 1989;**79**: 1077–1083.
31. Montague, T.J., E.R. Smith, D.A. Cameron, et al., Isointegral analysis of body surface maps: surface distribution and temporal variability in normal subjects. *Circulation*, 1981;**63**: 1166–1172.
32. Flaherty, J.T., S.D. Blumenschein, A.W. Alexander, et al., Influence of respiration on recording cardiac potentials. Isopotential surface-mapping and vectorcardiographic study. *Am. J. Cardiol*., 1967;**20**: 21–28.
33. Spach, M.S., R.C. Barr, D.W. Benson, A.H. Walston, R.B. Warren, and S.B. Edwards, Body surface low-level potentials during ventricular repolarization with analysis of the ST segment. Variability in normal subjects. *Circulation*, 1979;**59**: 822–36.
34. Corlan, A.D., P.W. Macfarlane, and L. De Ambroggi, Gender differences in stability of the instantaneous patterns of body surface potentials during ventricular repolarisation. *Med. Biol. Eng. Comput*., 2003;**41**: 536–542.
35. Abildskov, J.A., A.K. Evans, R.L. Lux, and M.J. Burgess Ventricular recovery properties and QRST deflection area in cardiac electrograms. *Am. J. Physiol*., 1981;**239**: H227–231.

36. Sano, T., Y. Sakamoto, M. Yamamoto, and F. Suzuki, The body surface U wave potentials, in *Progress in Electrocardiology*, P.W. Macfarlane, Editor. Tunbridge Wells: Pitman Medical, 1979, pp. 227–231.
37. L. De Ambroggi, E. Locati, T. Bertoni, E. Monza, and P.J. Schwartz, Body surface potentials during T-U interval in patients with the idiopathic long QT syndrome, in *Clinical Aspects of Ventricular Repolarization*, chapter 47, G.S. Butrous and P.J. Schwartz, Editors. London: Farrand Press, 1989, pp. 433–436.
38. L. De Ambroggi, M. Besozzi, and B. Taccardi, Aspetti qualitativi e quantitativi delle elettromappe cardiache nell'infarto miocardico anteriore e inferiore. *G. Ital. Cardiol.*, 1974;**4**: 540–553.
39. L. De Ambroggi, T. Bertoni, C. Rabbia, and M. Landolina, Body surface potential maps in old inferior myocardial infarction. Assessment of diagnostic criteria. *J. Electrocardiol.*, 1986;**19**: 225–234.
40. L. De Ambroggi, T. Bertoni, M.L. Breghi, M. Marconi, and M. Mosca, Diagnostic value of body surface potential mapping in old anterior non-Q myocardial infarction. *J. Electrocardiol.*, 1988;**21**: 321–329.
41. Flowers, N.C., L.G. Horan, and J.C. Johnson, Anterior infarctional changes occurring during mid and late ventricular activation detectable by surface mapping techniques. *Circulation*, 1976;**54**: 906–913.
42. Flowers, N.C., L.G. Horan, G.S. Sohi, R.C. Hand, and J.C. Johnson, New evidence for infero-posterior myocardial infarction on surface potential maps. *Am. J. Cardiol.*, 1976;**38**: 576–581.
43. Vincent, G.M., J.A. Abildskov, M.J. Burgess, K. Millar, R.L. Lux, and R.F. Wyatt, Diagnosis of old inferior myocardial infarction by body surface isopotential mapping. *Am. J. Cardiol.*, 1977;**39**: 510–515.
44. H. Pham-Huy, R.M. Gulrajani, F.A. Roberge, R.A. Nadeau, G.E. Mailloux, and P. Savard, A comparative evaluation of three different approaches for detecting body surface isopotential map abnormalities in patients with myocardial infarction. *J. Electrocardiol.*, 1981;**14**: 43–55.
45. Toyama, S., K. Suzuki, M. Koyama, K. Yoshino, and K. Fujimolo, The body surface isopotential mapping of the QRS wave in myocardial infarction: comparative study of the scintigram with thallium-201. *J. Electrocardiol.*, 1982;**15**: 241–247.
46. Ohta, T., A. Kinoshita, J. Ohsugi, et al., Correlation between body surface isopotential maps and left ventriculograms in patients with old inferoposterior myocardial infarction. *Am. Heart J.*, 1982;**104**: 1262–1270.
47. Osugi, J. T. Ohta, J. Toyama, F. Takatsu, T. Nagaya, and K. Yamada, Body surface isopotential maps in old inferior myocardial infarction undetectable by 12 lead electrocardiogram. *J. Electrocardiol.*, 1984;**17**: 55–62.
48. Hirai, M., T. Ohta, A. Kinoshita, J. Toyama, T. Nagaya, and K. Yamada, Body surface isopotential maps in old anterior myocardial infarction undetectable by 12-lead electrocardiograms. *Am. Heart J.*, 1984;**108**: 975–982.
49. Kubota, I., M. Yamaki, K Ikeda, I. Yamaguchi, I. Tonooka, K. Tsuiki, and S. Yasui, Abnormalities of early depolarization in patients with remote anterior myocardial infarction and ventricular septal hypoperfusion. Diagnosis of septal MI BSM. *J. Electrocardiol.*, 1990;**23**: 307–313.
50. Hayashi, H., M. Hirai, A. Suzuki, et al., Correlation between various parameters derived from body surface maps and ejection fraction in patients with anterior myocardial infarction. *J. Electrocardiol.*, 1993;**26**: 17–24.
51. Suzuki, A., M. Hirai., H. Hayashi, et al. The ability of QRST isointegral maps to detect myocardial infarction in the presence of simulated left bundle branch block. *Eur. Heart J.*, 1993;**14**: 1094–1101.
52. Medvegy, M., I. Preda, P. Savard, et al., A new body surface isopotential map evaluation method to detect minor potential losses in non-Q wave myocardial infarction. *Circulation*, 2000;**101**: 1115–1121.
53. Medvegy, M., P. Savard, A. Pinter, et al., Simple, quantitative body surface potential map parameters in the diagnosis of remote Q wave and non-Q wave myocardial infarction. *Can. J. Cardiol.*, 2004;**20**: 1109–1115.
54. Corlan, A.D. and L. De Ambroggi, New quantitative methods of ventricular repolarization analysis in patients with left ventricular hypertrophy. *Ital. Heart J.*, 2000;**1**: 542–548.
55. Corlan, A.D., B.M. Horacek, and L. De Ambroggi, Prognostic value for ventricular tachicardia of indices of ventricular repolarization in patients with and without myocardial infarction. 32nd Congress of International Society of Electrocardiology. *Folia Cardiol.*, 2005;12(Suppl C): 52.
56. Muller, J.E., P.R. Maroko, and E. Braunwald, Precordial electrocardiographic mapping. A technique to assess the efficacy of interventions designed to limit infarct size. *Circulation*, 1978;**57**: 1–18.
57. Maroko, P.R., P. Libby, J.W. Covell, B.E. So bel, J. Ross Jr, and E. Braunwald, Precordial S-T segment elevation mapping. An atraumatic method for assessing alterations in the extent of myocardial ischemic injury. *Am. J. Cardiol.*, 1972;**29**: 223–230.
58. Muller, J.E., P.R. Maroko, and E. Braunwald, Evaluation of precordial electrocardiographic mapping as a means of assessing changes in myocardial ischemic injury. *Circulation*, 1975;**52**: 16–27.
59. Holland, R.P. and H. Brooks, TQ-ST segment mapping: critical review and analysis of current concepts. *Am. J. Cardiol.*, 1977;**40** 110–129.
60. Surawicz, S., The disputed S-T segment mapping: is the technique ready for wide application in practice? *Am. J. Cardiol.*, 1977;**40**: 137–140.
61. Mirvis, D.M., Body surface distributions of repolarization forces during acute myocardial infarction. I. Isopotential and isoarea mapping. *Circulation*, 1980: **62**: 878–887.
62. Montague, T.J., E.R. Smith, C.A. Spencer, et al., Body surface electrocardiographic mapping in inferior myocardial infarction. Manifestation of left and right ventricular involvement. *Circulation*, 1983: **67**: 665–673.
63. Menown, I.B.A., J. Allen, J. McC Anderson, and A.A.J. Adgey, Early diagnosis of right ventricular or posterior infarction associated with inferior wall left ventricular acute myocardial infarction. *Am. J. Cardiol.*, 2000;**85**: 934–938.
64. McClelland, A.J.J., C.G. Owens, I.B. Menown, M. Lown, and A.A. Adgey, Comparison of 80-lead body surface map to physician and to 12-lead electrocardiogram in detection of acute myocardial infarction. *Am. J. Cardiol.*, 2003;**92**: 252–257.
65. Maynard, S.J., I.B. Menown, G. Manoharan, J. Allen, J. McC Anderson, and A.A. Adgey, Body surface mapping improves early diagnosis of acute myocardial infarction in patients with chest pain and left bundle branch block. *Heart*, 2003;**89**: 998–1002.

66. De Ambroggi, L., E. Macchi, B. Brusoni, and B. Taccardi, Electromaps during ventricular recovery in angina patients with normal resting ECG. *Adv. Cardiol*., 1977;**19**: 88–90.
67. Stilli, D., E. Musso, E. Macchi, et al., Body surface potential mapping in ischemic patients with normal resting ECG. *Can. J. Cardiol*., 1986;Suppl A: 107–112A.
68. Kornreich, F., P. Block P, and D. Brismee, The missing waveform information in the orthogonal electrocardiogram (Frank leads). Ill. Computer diagnosis of angina pectoris from "maximal" QRS surface waveform information at rest. *Circulation*, 1974;**49**: 1212–1222.
69. Spekhorst, H., A. Sippens-Groenewegen, G.K. David, M.J. Janse, and A.J. Dunning, Body surface mapping during percutaneous transluminal coronary angioplasty. QRS changes indicating regional myocardial conduction delay. *Circulation*, 1990;**81**: 840–849.
70. Shenasa, M., D. Hamel, J. Nasmith, et al., Body surface potential mapping of ST segment shift in patient undergoing percutaneous transluminal coronary angioplasty. *J. Electrocardiol*., 1993;**26**: 43–51.
71. Cahyadi, Y.H., N. Takekoshi, and S. Matsui, Clinical efficacy of PTCA and identification of restenosis: evaluation by serial body surface potential mapping. *Am. Heart J*., 1991;**121**: 1080–1087.
72. Fox, K.M., A.P. Selwyn, and J.P.A. Shillingford, method for precordial surface mapping of the exercise electrocardiogram. *Br. Heart J*., 1978: 40: 1339–1343.
73. Fox, K., A. Selwyn, and J. Shillingford, Precordial electrocardiographic mapping after exercise in the diagnosis of coronary artery disease. *Am. J. Cardiol*., 1979;**43**: 541–546.
74. Mirvis, D.M., F.W. Keller Jr., J.W. Cox Jr., D.G. Zetlergren, R.F. Dowdie, and R.E. Ideker, Left precordial isopotential mapping during supine exercise. *Circulation*, 1977;**56**: 245–252.
75. Mirvis, D.M., Body surface distribution of exercise-induced QRS changes in normal subjects. *Am. J. Cardiol*., 1980: **46** 988–996.
76. Miller, W.T. III, M.S. Spach, and R.B. Warren, Total body surface potential mapping during exercise: QRS- T-wave changes in normal young adults. *Circulation*, 1980;**62**: 632–645.
77. Simoons, M.L. and P. Block, Toward the optimal lead system and optimal criteria for exercise electrocardiography. *Am. J. Cardiol*., 1981;**47**: 1366–1374.
78. Wada, M., K. Kaneko, H. Teshigawara, et al., Exercise stress body surface isopotential map in patients with coronary artery disease: comparison with coronary angiographic and stress myocardial perfusion scintigraphic findings. *Jpn. Circ. J*., 1981;**45**: 1203–1207.
79. Yanowitz, F.G., G.M. Vincent, R.L. Lux, M. Merchant, L.S. Green, and J.A. Abildskov, Application of body surface mapping to exercise testing: S-T80 isoarea maps in patients with coronary artery disease. *Am. J. Cardiol*., 1982;**50**: 1109–1113.
80. Blumenschein, S.D., M.S. Spach, J.P. Boineau, et al., Genesis of body surface potentials in varying types of right ventricular hypertrophy. *Circulation*, 1968;**38**: 917–932.
81. Sohi, G.S., E.W. Green, N.C. Flowers, O.F. McMartin, and R.R. Masdcn, Body surface potential maps in patients with pulmonic valvular and aortic valvular stenosis of mild to moderate severity. *Circulation*, 1979;**59**: 1277–1283.
82. Holt, J.H. Jr, A.C.L. Barnard, and J.O. Kramer Jr., Multiple dipole electrocardiography: a comparison of electrically and angiographically determined left ventricular masses. *Circulation*, 1978;**57**: 1129–1133.
83. Yamaki, M., K. Ikeda, I. Kubota, K. Nakamura, K. Hanashima, K. Tsuiki, and S. Yasui, Improved diagnostic performance on the severity of left ventricular hypertrophy with body surface mapping. *Circulation*, 1989;**79**: 312–323.
84. Kornreich, F., T.J. Montague, P.M. Rautahariu, M. Kavadias, M.B. Horacek, and B. Taccardi, Diagnostic body surface potential map patterns in left ventricular hypertrophy during PQRST. *Am. J. Cardiol*., 1989;**63**: 610–617.
85. Hirai, M., H. Hayashi, Y. Ichihara, et al., Body surface distribution of abnormally low QRST areas in patients with left ventricular hypertrophy. An index of repolarization abnormalities. *Circulation*, 1991;**84**: 1505–1515.
86. Taccardi, B., L. De Ambroggi, and D. Riva, Chest maps of heart potentials in right bundle branch block. *J. Electrocardiol*., 1969;**2**: 109–116.
87. Sugenoya, J., S. Sugiyama, M. Wada, N. Niimi, H. Oguri, J. Toyama, and K. Yamada, Body surface potential distribution following the production of right bundle branch block in dogs: effects of breakthrough and right ventricular excitation on the body surface potentials. *Circulation*, 1977;**55**: 49–54.
88. Sugenoya, J., Interpretation of the body surface isopotential maps of patients with right bundle branch block. Determination of the region of the delayed activation within the right ventricle. *Jpn. Heart J*., 1978;**19**: 12–27.
89. Preda, I., I. Bukosza, G. Kozmann, Y.V. Shakin, A. Szèkely, and Z. Antalòczy, Surface potential distribution on the human thoracic surface in the left bundle branch block. *Jpn. Heart J*., 1979;**20**: 7–21.
90. Musso, E., D. Stilli, E. Macchi, et al., Body surface maps in left bundle branch block uncomplicated or complicated by myocardial infarction, left ventricular hypertrophy or myocardial ischemia. *J. Electrocardiol*., 1987;**20**: 1–20.
91. Sohi, G.S., N.C. Flowers, L.G. Boran, M.R. Sridharan, and J.C. Johnson, Comparison of total body surface map depolarization patterns of left bundle branch block and normal axis with left bundle branch block and left axis deviation. *Circulation*, 1983;**67**: 660–664.
92. Preda, I., Z. Antaloczy, I. Bukosza, G. Kozmann, and A. Szckely, New elcctrocardiological infarct criteria in the presence of left bundle branch block (surface mapping study), in *Progress in Electrocardiology*, P.W. Macfarlane, Editor. Tunbridge Wells: Pitman Medical, 1979, pp. 231–235.
93. Gallagher, J.J., A.R. Ticzon, A.G. Wallace, and J. Kasell, Activation studies following experimental hemiblock in the dog. *Circ. Res*., 1974;**35**: 752–763.
94. Sohi, G.S. and N.C. Flowers, Effects of left anterior fascicular block on the depolarization process as depicted by total body surface mapping. *J. Electrocardiol*., 1980: **13**: 143–152.
95. Yamada, K., J. Toyama, M. Wada, et al., Body surface isopotential mapping in Wolff-Parkinson-White syndrome. Noninvasive method to determine the location of the accessory atrioventricular pathway. *Am. Heart J*., 1975;**90**: 721–734.
96. De Ambroggi, L., B. Taccardi, and E. Macchi, Body-surface maps of heart potentials. Tentative localization of pre-excited areas in forty-two Wolff-Parkinson-White patients. *Circulation*, 1976;**54**: 251–263.
97. Spach, M.S., R.C. Ban, and C.F. Lanning, Experimental basis for QRS and T wave potentials in the WPW syndrome. The relation of epicardial to body surface potential distributions in the intact chimpanzee. *Circ. Res*., 1978;**42**: 103–118.

98. Iwa, T. and T. Magara, Correlation between localization of accessory conduction pathway and body surface maps in the Wolff-Parkinson. While syndrome. *Jpn. Circ. J.*, 1981;**45**: 1192–1198.
99. Benson, D.W. Jr., R. Sterba, J.J. Gallagher, A. Walston II, and M.S. Spach, Localization of the site of ventricular preexcitation with body surface maps in patients with Wolff-Parkinson-White: syndrome. *Circulation*, 1982;**65**: 1259–1268.
100. Kamakura, S., K. Shimomura, T. Ohe, M. Matsuhisa, and H. Yoyoshima, The role of initial minimum potential on body surface maps in predicting the site of accessory pathways in patients with Wolff-Parkinson-White syndrome. *Circulation*, 1986;**74**: 89–96.
101. Liebman, J., J.A. Zeno, B. Olshansky, et al., Electrocardiographic body surface potential mapping in the Wolff-Parkinson-White syndrome. Noninvasive determination of the ventricular insertion sites of accessory atrioventricular connections. *Circulation*, 1991;**83**: 886–901.
102. Dubuc, M., R. Nadeau, G. Tremblay, T. Kus, F. Molin, and P. Savard, Pace mapping using body surface potential maps to guide catheter ablation of accessory pathways in patients with Wolff-Parkinson-White syndrome. *Circulation*, 1993;**87**: 135–143.
103. Frank, E., Electric potential produced by two point current sources in a homogeneous conducting sphere. *J. Appl. Physiol.*, 1952;**23**: 1225–1228.
104. De Ambroggi, L. and B. Taccardi, Current and potential fields generated by two dipoles. *Circ. Res.*, 1970;**27**: 901–911.
105. Knippel, M., D. Pioselli, F. Rovelli, L. Campolo, E. Panzeri, and A. Pellegrini, Tachicardie ribelli nella sindrome da preeccitazione: trattamento chirurgico di cinque casi. *G. Ital. Cardiol.*, 1974;**4**: 657.
106. Guiraudon G.M., G.J. Klein, S. Gulamhusein, et al., Surgery for Wolff-Parkinson-White syndrome: further experience with epicardial approach. *Circulation*, 1986;**74**: 525–529.
107. Sippens-Groenewegen, A., H. Spekhorst, N.M. van Hemel, et al., Body surface mapping of ectopic left and right ventricular activation. QRS spectrum in patients without structural heart disease. *Circulation*, 1990;**82**: 879–896.
108. Sippens-Groenewegen, A., H. Spekhorst, N.M. van Hemel, et al., Localization of the site of origin of postinfarction ventricular tachycardia by endocardial pace mapping. Body surface mapping compared with the 12-lead electrocardiogram. *Circulation*, 1993;**88**: 2290–2306.
109. Sippens-Groenewegen, A, H. Spekhorst, N.M. van Hemel, et al., Value of body surface mapping in localizing the site of origin of ventricular tachycardia in patients with previous myocardial infarction. *J. Am. Coll. Cardiol.*, 1994;**24**: 1708–1724.
110. McClelland, A.J.J., C.G. Owens, C. Navarro, B. Smith, M.J.D. Roberts, J. Anderson, and A.A.J. Adgey, Usefulness of body surface maps to demonstrate ventricular activation patterns during left ventricular pacing and reentrant activation during ventricular tachycardia in men with coronary heart disease and left ventricular dysfunction. *Am J Cardiol* 2006;**98**: 591–596.
111. Lux, R.L., A.K. Evans, M.J. Burgess, R.F. Wyatt, and J.A. Abildskov, Redundancy reduction for improved display and analysis of body surface potential maps. I. Spatial compression. *Circ. Res.*, 1981;**49**: 186–196.
112. Bertoni, T., M.L. Breghi, M. Marconi, G. Bonifaccio, and L. De Ambroggi, Usefulness of the QRST integral maps to detect vulnerability to malignant arrhythmias in patients with old myocardial infarction, in *Electrocardiology '87*, E. Schubert, Editor. Berlin: Akademie-Verlag, 1988, pp. 247–250.
113. Abildskow, J.A., L.S. Green, and R.L. Lux, Detection of disparate ventricular repolarization by means of the body surface electrocardiogram, in*Cardiac Electrophysiology and Arrhythmias*, D.P. Zipes and J. Jalife, Editors. Orlando: Grune & Stratton, 1985, pp. 495–499.
114. Hubley-Kozey, C.L., B.L. Mitchell, M.J. Gardner, J.W. Warren, C.J. Penney, E.R. Smith, and B.M. Horacek, Spatial features in body-surface potential maps can identify patients with a history of sustained ventricular tachycardia. *Circulation*, 1995;**92**: 1825–1838.
115. Korhonen, P., T. Husa, T. Konttila, I. Tierala, M. Makijarvi, H. Vaananen, and L. Toivonen, Complex T-wave morphology in body surface mapping in prediction of arrhythmic events in patients with acute myocardial infarction and cardiac dysfunction. *Europace* 2009;**11**: 514–520.
116. Faugère, G., P. Savard, R.A. Nadeau, D. Derome, M. Shenasa, P.L. Page, and R. Guardo, Characterization of the spatial distribution of late ventricular potentials by body surface mapping in patients with ventricular tachycardia. *Circulation*, 1986;**74**: 1323–1333.
117. Shibata, T., I. Kubota, K. Ikeda, K. Tsuiki, and S. Yasui, Body surface mapping of high-frequency components in the terminal portion during QRS complex for the prediction of ventricular tachycardia in patients with previous myocardial infarction. *Circulation*, 1990;**82**: 2084–2092.
118. De Ambroggi, L., T. Bertoni, E. Locati, M. Stramba-Badiale, and P.J. Schwartz, Mapping of body surface potentials in patients with the idiopathic long QT syndrome. *Circulation*, 1986;**74**: 1334–1345.
119. De Ambroggi, L., M.S. Negroni, E. Monza, T. Bertoni, and P.J. Schwartz, Dispersion of ventricular repolarization in the long QT syndrome. *Am. J. Cardiol.*, 1991;**68**: 614–620.
120. De Ambroggi, L., E. Aimè, C. Ceriotti, M. Rovida, and S. Negroni, Mapping of ventricular repolarization potentials in patients with arrhythmogenic right ventricular dysplasia: principal component analysis of the ST-T waves. *Circulation*, 1997;**96**: 4314–4318.
121. Peeters, H.A., A. SippensGroenewegen, B.A. Schoonderwoerd, E.F. Wever, C.A. Grimbergen, R.N. Hauer, and E.O. Rohles de Medina, Body-surface QRST integral mapping. Arrhythmogenic right ventricular dysplasia versus idiopathic right ventricular tachycardia. *Circulation*, 1997;**95**: 2668–2676.
122. Antzelevitch, C., P. Brugada, M. Borggrefe, et al., Brugada syndrome: report of the second consensus conference. *Circulation*, 2005;**111**: 659–670.
123. Bruns, H.J., L. Eckardt, C. Vahlhaus, E. Schulze-Bahr, W. Haverkamp, M. Borggrefe, G. Breithardt, and T. Wichter, Body surface potential mapping in patients with Brugada syndrome: right precordial ST segment variations and reverse changes in left precordial leads. *Cardiovasc. Res.*, 2002;**54**: 58–66.
124. Eckardt, L., H.J. Bruns, M. Paul, P. Kirchhof, E. Schulze-Bahr, T. Wichter, G. Breithardt, M. Borggrefe, and W. Haverkamp, Body surface area of ST elevation and the presence of late potentials correlate to the inducibility of ventricular tachyarrhythmias in Brugada syndrome. *J. Cardiovasc. Electrophysiol.*, 2002;**13**: 742–749.
125. Hisamatsu, K., K.F. Kusano, H. Morita, S. Takenaka, S. Nagase, K. Nakamura, T. Emori, H. Matsubara, and T. Ohe, Usefulness of body surface mapping to differentiate patients with Brugada

syndrome from patients with asymptomatic Brugada syndrome. *Acta Med. Okayama*, 2004;**58**: 29–35.

126. Lux, R.L., C.R. Smith, R.F. Wyatt, and J.A. Abildskov, Limited lead selection for estimation of body surface potential maps in electrocardiography. *IEEE Trans. Biomed. Eng.*, 1978;**25**: 270–276.
127. Taccardi, B., C. Viganotti, E. Macchi, and L. De Ambroggi, Relationships between the current field surrounding an isolated dog heart and the potential distribution on the surface of the body. *Adv. Cardiol.*, 1976;**16**: 72–76.
128. Abildskov, J.A., M.J. Burgess, K. Millar, G.M. Vincent, R.F. Wyatt, and R.L. Lux, Distribution of body surface potentials with experimentally-induced multiple cardiac generators. *Adv. Cardiol.*, 1974;**10**: 69–76.
129. Spach, M.S., R.C. Barr, C.F. Lanning, and P.C. Tucek, Origin of body surface QRS and T wave potentials from epicardial potential distributions in the intact chimpanzee. *Circulation*, 1977;**55**: 268–278.
130. Spach, M.S., R.C. Barr, and C.F. Lanning, Experimental basis for QRS and T wave potentials in the WPW syndrome. The relation of epicardial to body surface potential distributions in the intact chimpanzee. *Circ. Res.*, 1978;**42**: 103–118.
131. Ramsey, M. III, R.C. Barr, and M.S. Spach, Comparison of measured torso potentials with those simulated from epicardial potentials for ventricular depolarization and repolarization in the intact dog. *Circ. Res.*, 1977;41: 660–672.
132. Barr, R.C. and M.S. Spach, Inverse calculation of QRS-T epicardial potentials from body surface potential distributions for normal and ectopic beats in the intact dog. *Circ. Res.*, 1978;**42**: 661–675.
133. Colli Franzone, P., L. Guerri, B. Taccardi, and C. Viganotti, A regularization method for inverse electrocardiology applied to data from an isolated dog heart experiment, in *Modern Electrocardiology*, Z. Antaloczy, Editor. Amsterdam: Excerpta Medica, 1978, pp. 75–80.
134. Oster, H.S., B. Taccardi, R.L. Lux, P.H. Ershler, and Y. Rudy, Noninvasive electrocardiographic imaging. Reconstruction of epicardial potentials, electrograms, and isochrones and localization of single and multiple electrocardiac events. *Circulation*, 1997;**96**: 1012–1024.
135. Burnes, J.E., B. Taccardi, and Y. Rudy, A Noninvasive electrocardiographic imaging modality for cardiac arrhythmias. *Circulation*, 2000;**102**: 2151–2158.
136. Burnes, J.E., B. Taccardi, P.H. Ershler, and Y. Rudy, Noninvasive electrocardiographic imaging of substrate and intramural ventricular tachycardia in infarcted hearts. *J. Am. Coll. Cardiol.*, 2001;**38**: 2071–2078.
137. Ghanem, R.N., J.E. Burnes, A.L. Waldo, and Y. Rudy, Imaging dispersion of myocardial repolarization, II. Noninvasive reconstruction of epicardial measures. *Circulation*, 2001;**104**: 1306–1312.
138. Ramanatham, C., R.N. Ghanem, P. Jia, K. Ryu, and Y. Rudy, Noninvasive electrocardiographic imaging for cardiac electrophysiology and arrhythmias. *Nat. Med.*, 2004;**10**: 422–428.
139. Ghanem, R.N., P. Jia, C. Ramanatham, K. Ryu, A. Markowitz, and Y. Rudy, Noninvasive electrocardiographic imaging (ECGI): comparison to intraoperative mapping in patients. *Heart Rhythm*, 2005;**2**: 339–354.
140. Intini, A., R.N. Goldstein, P. Jia, C. Ramanathan, K. Ryu, B. Giannattasio, R. Gilkeson, B.S. Stambler, P. Brugada, W.G. Stevenson, Y. Rudy, and A.L. Waldo, Electrocardiographic imaging (ECGI), a novel diagnostic modality used for mapping of focal left ventricular tachycardia in a young athlete. *Heart Rhythm*. 2005;**2**: 1250–1252.
141. Wang, Y., P.S. Cuculich, P.K. Woodard, B.D. Lindsay, and Y. Rudy, Focal atrial tachycardia after pulmonary vein isolation: Noninvasive mapping with electrocardiographic imaging (ECGI). *Heart Rhythm* 2007;**4**: 1081–1084.
142. Van Dam, P.M., T.F. Oostendorp, A.C. Linnenbank, and A. van Oosterom, Non-invasive imaging of cardiac activation and recovery. *Ann Biomed Eng* 2009;**37**: 1739–1756.